

Synthetic Stellar Photometry - II. Testing the bolometric flux scale, and tables of bolometric corrections for the Hipparcos/Tycho, Pan-STARRS1, SkyMapper and *JWST* systems.

L. Casagrande^{1,2*}, Don A. Vandenberg³

¹ *Research School of Astronomy and Astrophysics, Mount Stromlo Observatory, The Australian National University, ACT 2611, Australia*

² *ARC Centre of Excellence for All Sky Astrophysics in 3 Dimensions (ASTRO 3D)*

³ *Department of Physics & Astronomy, University of Victoria, P.O. Box 1700 STN CSC, Victoria, BC, V8W 2Y2, Canada*

Received; accepted

ABSTRACT

We use MARCS model atmosphere fluxes to compute synthetic colours, bolometric corrections and reddening coefficients for the Hipparcos/Tycho, Pan-STARRS1, SkyMapper and *JWST* systems. Tables and interpolation subroutines are provided to transform isochrones from the theoretical to various observational planes, to derive bolometric corrections, synthetic colours and colour-temperature relations at nearly any given point of the HR diagram for $2600\text{ K} \leq T_{\text{eff}} \leq 8000\text{ K}$, and different values of reddening in 85 photometric filters. We use absolute spectrophotometry from the CALSPEC library to show that bolometric fluxes can be recovered to ~ 2 percent from bolometric corrections in a single band, when input stellar parameters are well known for FG dwarfs at various metallicities. This sole source of uncertainty impacts interferometric T_{eff} to ≈ 0.5 percent (or 30 K at the solar temperature). Uncertainties are halved when combining bolometric corrections in more bands, and limited by the fundamental uncertainty of the current absolute flux scale at 1 percent. Stars in the RAVE DR5 catalogue are used to validate the quality of our MARCS synthetic photometry in selected filters across the optical and infrared range. This investigation shows that extant MARCS synthetic fluxes are able to reproduce the main features observed in stellar populations across the Galactic disc.

Key words: techniques: photometric — stars: atmospheres — stars: fundamental parameters — stars: Hertzsprung-Russell and colour-magnitude diagrams — (Galaxy:) globular clusters: general

1 INTRODUCTION

Synthetic stellar photometry is crucial for the translation of theoretical stellar quantities, namely effective temperatures (T_{eff}), surface gravities ($\log g$), metallicities ($[\text{Fe}/\text{H}]$ often together with $[\alpha/\text{Fe}]$) and luminosities into observables such as magnitudes and colours in different photometric systems. With the advent of large scale photometric surveys, this is becoming increasingly important, in order to allow comparisons of observed stellar populations with theoretical stellar models, to derive e.g., stellar ages, star-formation histories, distances etc. . . . The Gaia mission is providing exquisite distances of stars, which then translate into precise absolute magnitudes (Gaia Collaboration et al. 2016). However, when comparing them with stellar models, one of the main limiting factors is the availability of bolometric corrections (BCs) to translate those magnitudes into luminosities.

In this paper we continue our effort to provide reliable syn-

thetic colours and BCs from the MARCS library of theoretical fluxes (Gustafsson et al. 2008) for different T_{eff} , $\log g$, $[\text{Fe}/\text{H}]$ and $[\alpha/\text{Fe}]$ combinations. We follow the approach of Casagrande & Vandenberg (2014, hereby Paper I), where detailed information on the MARCS flux library, and the main concepts of synthetic photometry can be found. Paper I also addresses one of the main limitation of synthetic colours computed from static 1D model atmospheres, namely microturbulent velocity, whose effect can be substantial in the blue and ultraviolet spectral region (see Chiavassa et al. 2018; Bonifacio et al. 2018, for an investigation of synthetic colours from 3D model atmospheres). Here, we extend Paper I to include photometric systems which underpin large scale surveys, and which will be increasingly used over the next several years. These are the Tycho system (i.e. the Tycho-2 catalogue, as described in Høg et al. 2000) which comprises 2.5 million of the brightest stars in the sky (all part of the Tycho-Gaia Astrometric Solution, Michalik et al. 2015; Lindegren et al. 2016); SkyMapper (a photometric survey of the entire southern sky, Wolf et al. 2018); Pan-STARRS1 (Panoramic Survey Telescope and Rapid Re-

* Email: luca.casagrande@anu.edu.au

sponse System in the northern hemisphere, Chambers et al. 2016) and the filters installed on the James Webb Space Telescope (Gardner et al. 2006). Together with the photometric systems explored in Paper I (Johnson-Cousins, SDSS, 2MASS, *HST*-ACS and *HST*-WFC3) our transformations provide one of the most extended set of homogeneously derived and tested BCs and synthetic colours available in the literature. Expanding from Paper, I we provide an explicit formulation to translate bolometric corrections in physical fluxes, and use a number of well calibrated flux standards from the CALSPEC library¹ to test the performances of our bolometric corrections. This is becoming increasingly relevant in the context of deriving reliable bolometric fluxes for interferometric targets (e.g., Karovicova et al. 2018). Further, we use stellar parameters from the RAVE DR5 survey (Kunder et al. 2017) to generate synthetic colours for $\sim 10^5$ stars, and compare them with the observed ones, to validate our synthetic photometry at different wavelengths, and over a wide range of stellar parameters. Star cluster fiducials in the Pan-STARRS1 system are also used to show how our synthetic photometry can be used together with theoretical stellar models to produce colour-magnitude diagrams (CMDs).

2 SYNTHETIC PHOTOMETRY

The main concepts of synthetic photometry, along with the rationale behind the Vega, AB and ST magnitude systems are discussed in Paper I. Here we adhere to the same nomenclature, and provide information on the filters transmission curves (Figure 1), zero-points and absolute calibrations used to compute synthetic colours and BCs for the systems reported in Table 1 (analogous to that in Paper I).

As in Paper I, we apply the Cardelli et al. (1989) parametrisation of the extinction law (A_λ) to synthetic spectra, in order to derive synthetic colours and bolometric corrections for different values of reddening $E(B - V)$, between 0 and 0.72. The Cardelli et al. (1989) law is described by a smooth power law in the range $0.3 - 3.3\mu\text{m}$, and for the sake of this work we extrapolate its applicability to the reddest *JWST*-NIRCam filters, i.e. up to $\approx 5\mu\text{m}$. This extrapolation is qualitatively supported by recent observations, but beyond this limit the use of a single power law breaks down, and the extinction law is characterised by emission features (e.g. Fritz et al. 2011). Hence, it is not possible to apply a simple parametrisation beyond this limit, but overall A_λ is rather constant when averaged over the wavelength range of a broad-band filter. Here, we assume that the Cardelli et al. (1989) law, which is parametrised as function of $x = 1/\lambda$, remains constant at A_{λ_x} longward of $\lambda_x = \frac{1}{0.21}\mu\text{m}$. Because this assumption does not capture the full complexity of the mid-infrared extinction, the effects of reddening given in our tables for the MIRI system only provide some guidance of how synthetic magnitudes and bolometric corrections will behave when $E(B - V) > 0$. *JWST*-MIRI filters centred on emission features might have different magnitudes, and indeed, a full characterisation of the extinction law in the mid-infrared will be one of the studies to be carried out by the *JWST*.

2.1 Hipparcos/Tycho

The Hipparcos catalogue contains photometry (and astrometry) for more than 100,000 stars measured with the H_P band (Perryman

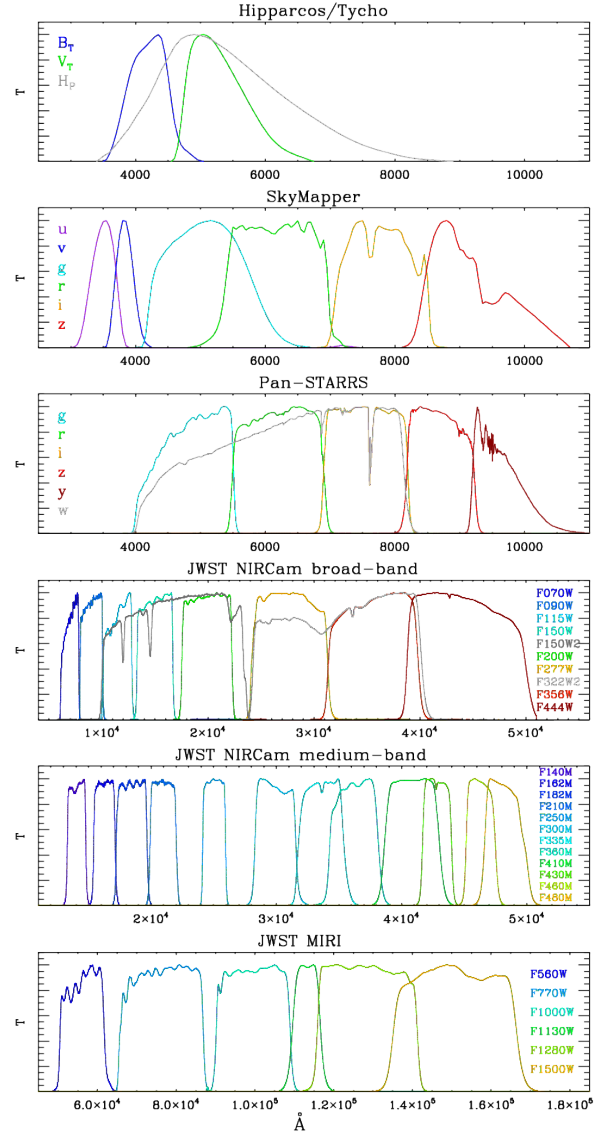


Figure 1. System response functions from which synthetic colours and bolometric corrections have been computed. All curves are normalised to one, and shown as a function of wavelength (in Å).

et al. 1997). In addition, for a much larger number of sources, a dichroic beam splitter on the Hipparcos satellite sent light onto two photomultiplier tubes, providing simultaneously measured B_T and V_T magnitudes. These are part of the Tycho-2 catalogue (*nota bene* the photometric system is called Tycho, but the catalogue is Tycho-2 being the second and final data-release, Høg et al. 2000) which contains photometry for 2.5 million stars. The Hipparcos and Tycho photometric systems and passbands are discussed in van Leeuwen et al. (1997), and have subsequently been revised by Bessell (2000) and Bessell & Murphy (2012). Here, we generate synthetic H_P , B_T , V_T adopting the AB formalism, with the passbands and zero-points provided by Bessell & Murphy (2012). Some limitations of the observed H_P , B_T and V_T magnitudes should be kept in mind. While these magnitudes are accurately and precisely calibrated over the entire sky for the bulk of stars, the quality of Tycho photometry quickly downgrades for $V_T \gtrsim 9$ (e.g., Ruchti et al.

¹ <http://www.stsci.edu/hst/observatory/crds/calspec.html>

Table 1. Characteristic parameters defining the photometric systems studied here. Refer to Paper I for the equations defining the VEGA, AB and ST system. The absolute calibration $\bar{f}_{\star,\zeta}$ is given in $\text{erg s}^{-1} \text{cm}^{-2} \text{\AA}^{-1}$. For each filter in *JWST*-NIRCam, the absolute calibration is provided for module A (left), B (centre) and averaged AB (right). See text for details.

Filter	T_ζ	VEGA system		AB system		ST system
		$m_{\star,\zeta}$	$\bar{f}_{\star,\zeta}$	ϵ_ζ	ϵ_ζ	ϵ_ζ
H_P	1	—	—	—	+0.030	—
B_T	1	—	—	—	+0.100	—
V_T	1	—	—	—	+0.037	—
u	2	—	—	—	0	—
v	2	—	—	—	0	—
g	2	—	—	—	0	—
r	2	—	—	—	0	—
i	2	—	—	—	0	—
z	2	—	—	—	0	—
g	3*	—	—	—	0	—
r	3*	—	—	—	0	—
i	3*	—	—	—	0	—
z	3*	—	—	—	0	—
y	3*	—	—	—	0	—
w	3*	—	—	—	0	—
$F070W$	4	0	1.6709E-09 / 1.6785E-09 / 1.6747E-09	0	0	0
$F090W$	4	0	8.2717E-10 / 8.3271E-10 / 8.2997E-10	0	0	0
$F115W$	4	0	3.9736E-10 / 3.9663E-10 / 3.9700E-10	0	0	0
$F150W$	4	0	1.5857E-10 / 1.5808E-10 / 1.5833E-10	0	0	0
$F150W2$	4	0	1.2708E-10 / 1.2712E-10 / 1.2710E-10	0	0	0
$F200W$	4	0	5.8441E-11 / 5.8466E-11 / 5.8454E-11	0	0	0
$F277W$	4	0	1.7519E-11 / 1.6905E-11 / 1.7228E-11	0	0	0
$F322W2$	4	0	1.0055E-11 / 1.0045E-11 / 1.0050E-11	0	0	0
$F356W$	4	0	6.5505E-12 / 6.5012E-12 / 6.5257E-12	0	0	0
$F444W$	4	0	2.9531E-12 / 2.8632E-12 / 2.9051E-12	0	0	0
$F140M$	4	0	1.9808E-10 / 1.9869E-10 / 1.9839E-10	0	0	0
$F162M$	4	0	1.1760E-10 / 1.1776E-10 / 1.1768E-10	0	0	0
$F182M$	4	0	7.5682E-11 / 7.5715E-11 / 7.5699E-11	0	0	0
$F210M$	4	0	4.7838E-11 / 4.7805E-11 / 4.7821E-11	0	0	0
$F250M$	4	0	2.4566E-11 / 2.4601E-11 / 2.4583E-11	0	0	0
$F300M$	4	0	1.2652E-11 / 1.2637E-11 / 1.2645E-11	0	0	0
$F335M$	4	0	8.1407E-12 / 8.0504E-12 / 8.0975E-12	0	0	0
$F360M$	4	0	6.0679E-12 / 6.0730E-12 / 6.0704E-12	0	0	0
$F410M$	4	0	3.8715E-12 / 3.7956E-12 / 3.8333E-12	0	0	0
$F430M$	4	0	3.1819E-12 / 3.1854E-12 / 3.1837E-12	0	0	0
$F460M$	4	0	2.3336E-12 / 2.3538E-12 / 2.3441E-12	0	0	0
$F480M$	4	0	2.0565E-12 / 1.9978E-12 / 2.0212E-12	0	0	0
$F560W$	5	0	1.1113E-12	0	0	0
$F770W$	5	0	3.4150E-13	0	0	0
$F1000W$	5	0	1.1908E-13	0	0	0
$F1130W$	5	0	7.1065E-14	0	0	0
$F1280W$	5	0	4.3917E-14	0	0	0
$F1500W$	5	0	2.3114E-14	0	0	0

An asterisk in the second column indicates that T_ζ given in the reference is already multiplied by λ and renormalised (see discussion in Section 2.2 of Paper I). **–1: Tycho.** Transmission curves from Bessell & Murphy (2012); ϵ_ζ values are obtained from their tables 3 and 5 (but with the opposite sign, following our definition of ϵ_ζ from Paper I). **–2: SkyMapper.** Transmission curves from Bessell et al. (2011), under the assumption that SkyMapper magnitudes are perfectly standardised on the AB system. **–3: Pan-STARRS1.** Transmission curves from Tonry et al. (2012) **–4: JWST-NIRCam.** Transmission curves available at <https://jwst-docs.stsci.edu/display/JTI/NIRCam+Filters> **–5: JWST-MIRI.** Transmission curves available at <http://ircamera.as.arizona.edu/MIRI/pces.htm>

2013, their figure 5). In addition, H_P photometry of the brightest stars (say $H_P \lesssim 1.5$) is likely affected by pulse pileup and should be used with caution (Bohlin 2014, their figure 6).

2.2 SkyMapper

SkyMapper is a 1.35m automated wide-field survey telescope located at Siding Spring Observatory (Australia), to carry a multi-epoch photometric survey of the entire southern sky to a final depth of ≈ 20 to ≈ 21 mag depending on the filters that are used. The

SkyMapper photometric system builds on the success of the *griz* filters used by the Sloan Digital Sky Survey (Fukugita et al. 1996), with the added value of the *uv* bands, designed to be strongly sensitive to stellar parameters. The SkyMapper *u* band mimics the Strömgren *u* filter, which is seated at the Balmer discontinuity, and provides good temperature sensitivity in hot stars, and gravity sensitivity across A, F and G spectral types. The SkyMapper *v* band is similar to the DDO38 filter, which is metallicity sensitive. A description and characterisation of the SkyMapper photometric system can be found in Bessell et al. (2011). The goal of SkyMapper is to map the entire southern sky in all six filters. Currently, Data Release 1 (DR1) is available, which covers more than 20,000 deg² and has more than 300 million unique sources. Further details on the survey, data quality and calibration are provided in Wolf et al. (2018). It should be appreciated that the standardisation of SkyMapper photometry to the AB system is still in progress. That is, while our synthetic magnitudes have been computed assuming perfect adherence to the AB system, small differences may be present in observed data. As a result, minor zero-point adjustments (ϵ_z) might be necessary to match observations. Therefore, when comparing predicted colours with published photometry from a given Data Release, the accompanying paper should be checked for information on potential zero-points departures from the AB system.

2.3 Pan-STARRS1

The Panoramic Survey Telescope & Rapid Response System (Pan-STARRS1) employs a 1.8m telescope at Haleakala Observatories (Hawaii) to image three quarters of the sky (3π Survey) in the visible and near infrared broad-band filters *grizy* (Chambers et al. 2016). A thorough discussion of the the Pan-STARRS1 photometric system is given in Tonry et al. (2012), who provide filter transmission curves, and detailed information on how to achieve standardisation to the AB magnitude system.

2.4 JWST

The James Webb Space Telescope (*JWST*) will be the premier infrared space observatory for the next decade (Gardner et al. 2006). The scientific instruments on board will allow imaging, spectroscopy and coronagraphy, covering a wide range of wavelengths from the edge of the visible to the mid-infrared. The two imaging instruments, the Near Infrared Camera (NIRCam, Rieke et al. 2005) and the Mid Infrared Instrument (MIRI, Rieke et al. 2015) will deliver high-precision and high-accuracy photometry across the 0.6 – 28 μ m range. At the present time, the system onto which *JWST* photometry will be standardised, and their zero-points, is not yet clear. Hence, in analogy to what is currently available for the *HST* (see Paper I), we have generated magnitudes in the VEGA, AB and ST systems also for *JWST* filters. The zero-points of the AB and ST systems are known by definition. (Standardising observations to the definition is the main observational challenge.) To derive zero-points for the VEGA system, we have used the latest absolute flux for α Lyr (Bohlin 2014) available from the CALSPEC library². While we expect that our synthetic photometry provides a realistic representation of future *JWST* observations, contaminations might still

occur to the optical telescope elements during deployment, thus changing the throughputs we have used here. Also, the standardisation of real data should be checked to determine whether any zero-point shifts should be applied onto our definitions.

2.4.1 NIRCam

NIRCam is *JWST*'s primary imager in the wavelength range 0.6 – 5 μ m. It consists of two, nearly identical modules, A and B, and offers 29 bandpass filters, covering extra-wide (W2), wide (W), medium (M) and narrow (N) bands. A description of each filter and their science goals can be found at <https://jwst-docs.stsci.edu/display/JTI/NIRCam+Filters>. We have generated colours and bolometric corrections for all but the narrow filters, using the total system throughputs. Throughputs vary somewhat between the 2 modules, especially at long wavelengths due to differences in detector quantum efficiencies. Thus, we have computed synthetic NIRCam photometry using module A, module B, and the average of the two (AB). The system response functions plotted in Figure 1 are for the AB case.

2.4.2 MIRI

The imaging mode for *JWST*'s MIRI offers 9 broad-band filters from 5.6 – 25.5 μ m. A description of each filter, and their purpose is available at <https://jwst-docs.stsci.edu/display/JTI/MIRI+Imaging>. Since MARCS synthetic fluxes extend only to 20 μ m, we have not computed synthetic photometry for filters redder than *F1500W* (Figure 1).

3 CONVERSION TO PHYSICAL FLUXES

In certain situations, it might be useful to transform a bolometric correction into a bolometric flux. For example, when the apparent magnitude of a star is known, and its angular diameter is measured, then knowledge of the bolometric flux allows a direct determination of its T_{eff} (e.g. Hanbury Brown et al. 1967). Alternatively, one might wish to know the bolometric flux of a star, to compare with luminosities predicted from stellar models if the distance is known. From the definition of bolometric correction in a given band ζ :

$$BC_{\zeta} = m_{\text{Bol}} - m_{\zeta} = M_{\text{Bol}} - M_{\zeta} \quad (1)$$

which is the same whether applied to apparent (lower case) or absolute (upper case) magnitudes. However, the zero-point of both apparent and absolute bolometric magnitudes is defined by the solar absolute bolometric magnitude ($M_{\text{Bol},\odot}$) and luminosity (L_{\odot}):

$$M_{\text{Bol}} = -2.5 \log \frac{L}{L_{\odot}} + M_{\text{Bol},\odot}. \quad (2)$$

We stress that while the solar luminosity L_{\odot} is a measured quantity, $M_{\text{Bol},\odot}$ is an arbitrary zero-point and any value is equally legitimate on the condition that once chosen, all bolometric corrections are scaled accordingly. To keep consistency with Paper I, our tables of bolometric corrections and interpolation routines are computed fixing $M_{\text{Bol},\odot} = 4.75$, and this value must be used in Eq. (1)–(3). It can be shown that the bolometric flux of a star having an observed magnitude m_{ζ} and bolometric correction BC_{ζ} is then:

$$f_{\text{Bol}} (\text{erg s}^{-1} \text{cm}^{-2}) = \frac{\pi L_{\odot}}{(1.296 \times 10^9 \text{ AU})^2} 10^{-0.4(BC_{\zeta} - M_{\text{Bol},\odot} + m_{\zeta} - 10)}$$

² Regularly updated absolute spectrophotometry can be found at <http://www.stsci.edu/hst/observatory/cdbs/calspec.html>. We have used the latest available at the time of this investigation, `alpha_lyr_stis_008.fits`.

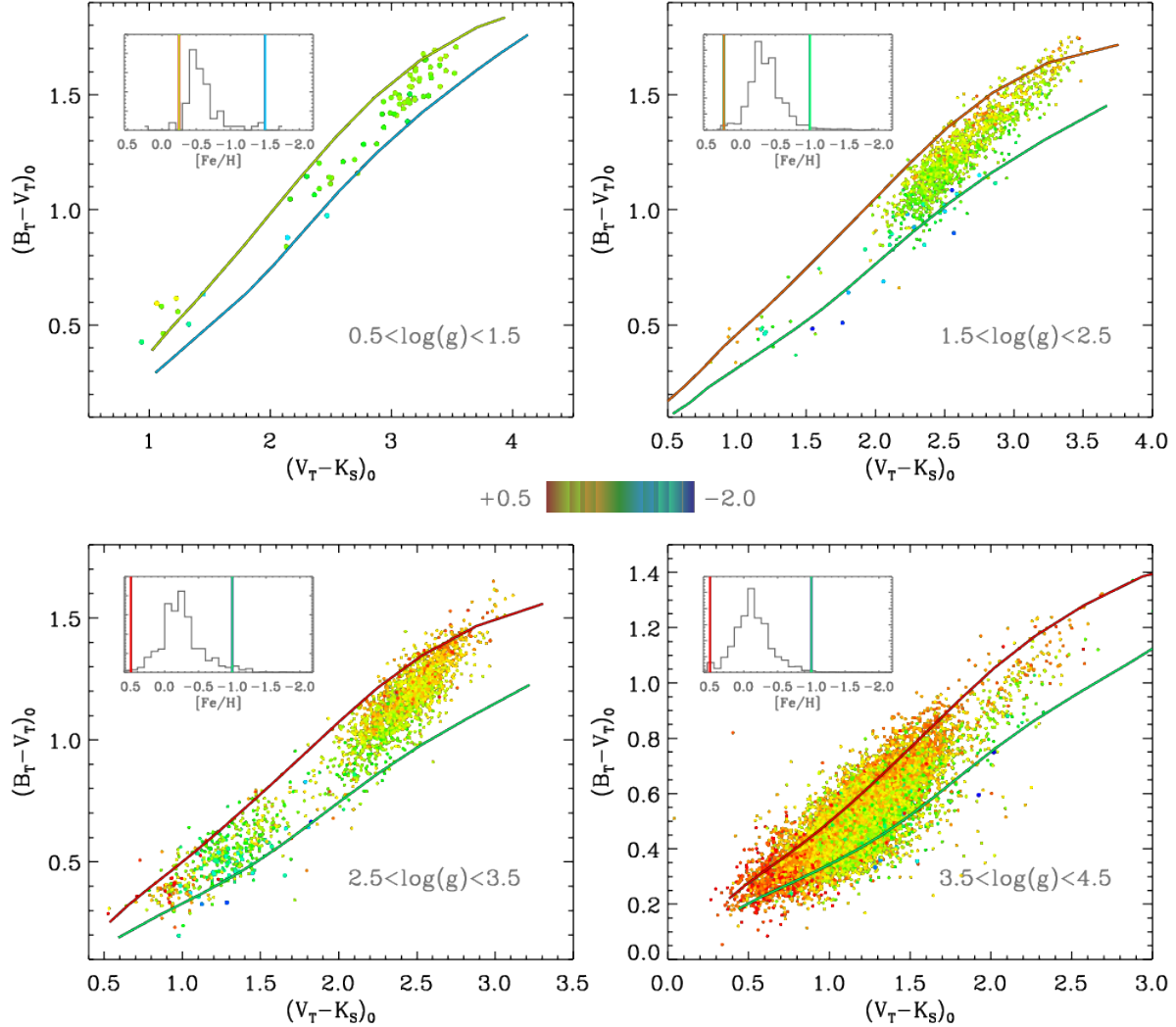


Figure 2. Colour-colour planes for stars in RAVE DR5 satisfying the quality cuts described in the text, and also having Tycho and 2MASS photometry. Each panel displays stars in the $\log g$ range indicated in the bottom right, coded by metallicity as indicated by the palette. Insets show the metallicity histogram within each panel. Continuous lines are synthetic colours predicted by MARCS models at metallicities broadly encompassing the sample (marked by vertical lines in histograms). $\log g$ of MARCS models is 1, 2, 4, 3 (clockwise from top-left). Only stars with photometric errors < 0.05 mag in each band are shown. Photometry has been dereddened using rescaled $E(B - V)$ values as described in the text.

$$\approx 8.358 \times 10^{-45} L_{\odot} 10^{-0.4(BC_{\zeta} - M_{\text{Bol},\odot} + m_{\zeta} - 10)}, \quad (3)$$

where we adopted $AU = 1.495978707 \times 10^{13}$ cm from the IAU 2012 Resolution B2, and L_{\odot} is the solar luminosity in erg s^{-1} . Note that the solar luminosity specified in IAU 2015 Resolution B3 is reduced by ≈ 0.4 percent with respect to older measurements³. Also worth mentioning is that, when deriving bolometric fluxes to compare with the predictions of a given set of stellar models, the same value of L_{\odot} that was assumed in the computation of those models

³ The relevant IAU Resolutions can be found at <https://www.iau.org/static/resolutions/IAU2012.English.pdf> <https://www.iau.org/static/resolutions/IAU2015.English.pdf>. These resolutions also recommend the adoption of $M_{\text{Bol},\odot} = 4.74$. If users wish to adopt this value, the BCs from our interpolation routines must be increased by -0.01 mag

should be used in Eq. (3) in order to obtain internal consistency. Finally, we recall that if a value of $E(B - V)$ is provided, our interpolation routines take into account the effect of reddening on bolometric corrections, which can then be directly used in Eq. (3). Alternatively, one could use bolometric corrections for no reddening, and deredden apparent magnitudes as $m_{\zeta} - R_{\zeta}E(B - V)$, using the extinction coefficients R_{ζ} tabulated in Table A1 of Paper I, and Table B1 in the Appendix (the first method is to be preferred because it automatically takes into account the dependence of extinction coefficients on stellar parameters, whereas using tabulated R_{ζ} is not as exact. See discussion in Paper I).

It might also be useful to deal with physical units in the case of infrared observations, where Jansky is often the adopted unit of measurement instead of magnitude. This might be relevant for the *JWST* filters, and the fact that we provide AB magnitudes readily allows for this conversion. From the definition of AB magnitudes, it

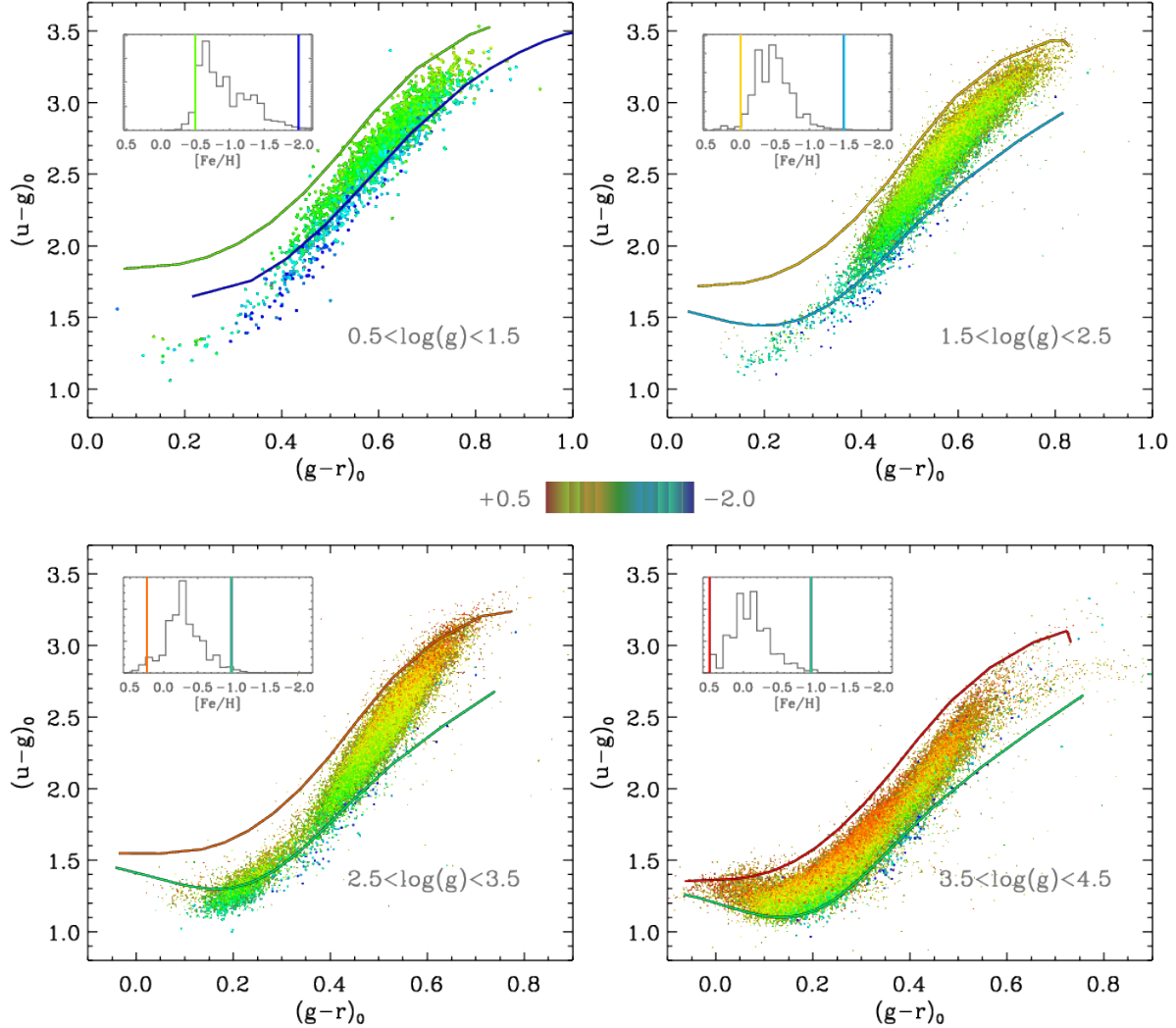


Figure 3. Same as Figure 2 but for combinations of SkyMapper colours. In addition to the RAVE quality cuts described in the main text, only stars with photometric errors < 0.05 mag in each band, no photometric flags, and `class.star` > 0.9 are shown. Photometry has been dereddened using rescaled $E(B - V)$.

follows that:

$$\bar{f}_\nu(Jy) = 3631 \times 10^{-0.4(m_{AB} - \epsilon_\zeta)}. \quad (4)$$

where m_{AB} is the AB magnitude for a given ζ filter and ϵ_ζ allows for zero-point offsets (with $\epsilon_\zeta = 0$ for a perfect standardisation to the AB system, see the discussion in Paper I).

4 COMPARISONS WITH OBSERVATIONS

Here we evaluate the performance of our BCs and synthetic colours in three different ways. The first method relies on having precise and accurate stellar parameters, observed magnitudes and absolute spectrophotometry (which is currently possible only for a limited number of stars) to check how well bolometric fluxes can be recovered. The second depends instead on having a statistically large sample of stars (of order 10^5) with overall well calibrated stellar parameters. In this case, comparisons of synthetic and observed colours in different bands for a wide range of T_{eff} , $\log g$

and $[\text{Fe}/\text{H}]$ test the combined performance of the MARCS model fluxes together with the standardisation, zero-points and system response functions that were adopted when we computed the synthetic photometry. In the third approach, we couple our BCs with stellar isochrones to examine the extent to which the stellar models are able to provide consistent interpretations of as many CMDs as possible that can be constructed from multi-colour observations of a given star cluster. Such analyses can provide valuable insights into both the temperatures of the stellar models and possible deficiencies of the synthetic colours. In all instances we have used the MARCS tables of BCs and interpolation routines made publicly available through this work, assuming standard $[\alpha/\text{Fe}]$ enhancements. As for Paper I, BC transformations for different α -enhancements can also be generated (see also Appendix A).

4.1 Testing the bolometric flux scale

The CALSPEC library contains composite stellar spectra that are flux standards on the *HST* system. The latter is based on three hot,

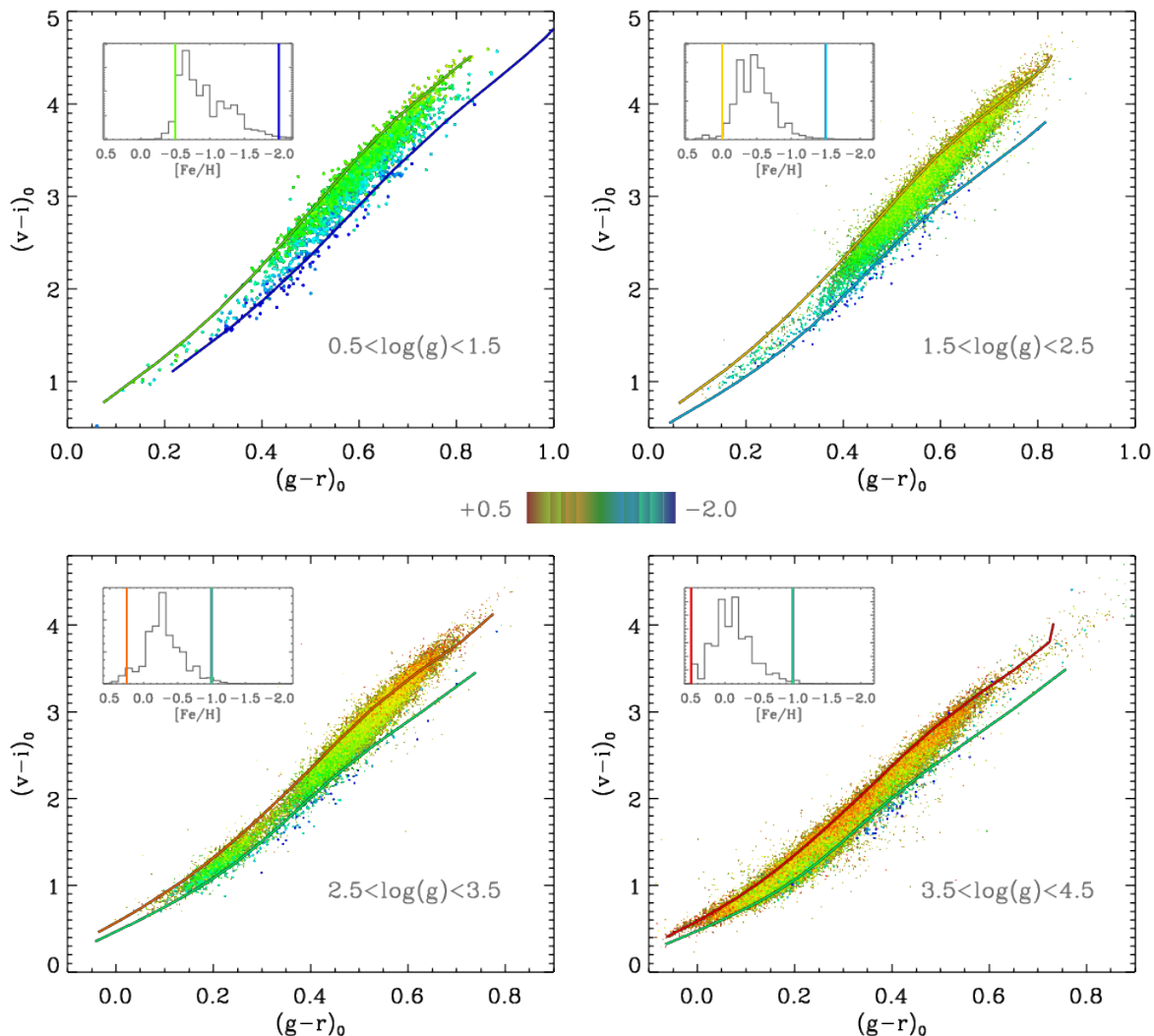


Figure 4. Same as Figure 3 but for a different combination of SkyMapper colours.

pure hydrogen white dwarf standards normalised to the absolute flux of Vega at 5556 Å. This spectrophotometry is expected to be accurate at the (few) percent level (Bohlin 2014).

Thus, CALSPEC absolute spectrophotometry currently provides the best way to test how well our bolometric corrections can recover stellar fluxes. In particular, the highest quality measurements in the CALSPEC library are those obtained by the STIS (0.17–1.01 μm) and NICMOS (1.01–2.49 μm) instruments on board of the *HST*.

Since our synthetic BCs are computed at a given T_{eff} , $\log g$, $[\text{Fe}/\text{H}]$ and $[\alpha/\text{Fe}]$, these quantities need to be known. Also, we want to consider stars with good photometry, no binary contamination, no dust emission, no reported variability and ideally little or no reddening. These requirements are met at different levels by a number of stars in the CALSPEC library, and for this reason we group them into three categories. A summary of all stars, their adopted parameters, CALSPEC bolometric fluxes and those we recover using our BCs is presented in Table 2. In what follows we briefly discuss each category.

4.1.1 Tier 1

Tier 1 stars are those with best possible parameters. In fact, only one star, HD209458, qualifies. It has both STIS and NICMOS spectrophotometry, meaning that almost 96 percent of its bolometric flux is directly measured. This star is a primary CALSPEC calibrator, and a proposed JWST primary flux standard (Gordon et al. 2009). Its stellar parameters are extremely well characterised, which then lead to a reliable estimate of its bolometric flux (del Burgo & Allende Prieto 2016). Also, this star is nearby (≈ 50 pc) and hence reddening free, and it has very good photometry in the Tycho (Høg et al. 2000) and 2MASS (Skrutskie et al. 2006) systems.

Using the BCs that are obtained by interpolations in our tables, we are usually able to recover the CALSPEC bolometric flux of this star to within ≈ 1 percent in each band. To account for the uncertainties associated with the bolometric fluxes so derived, we ran MonteCarlo simulations that take into account the quoted uncertainties in both the input stellar parameters and the observed photometry. This source of uncertainty amounts to of order 2 percent in each band.

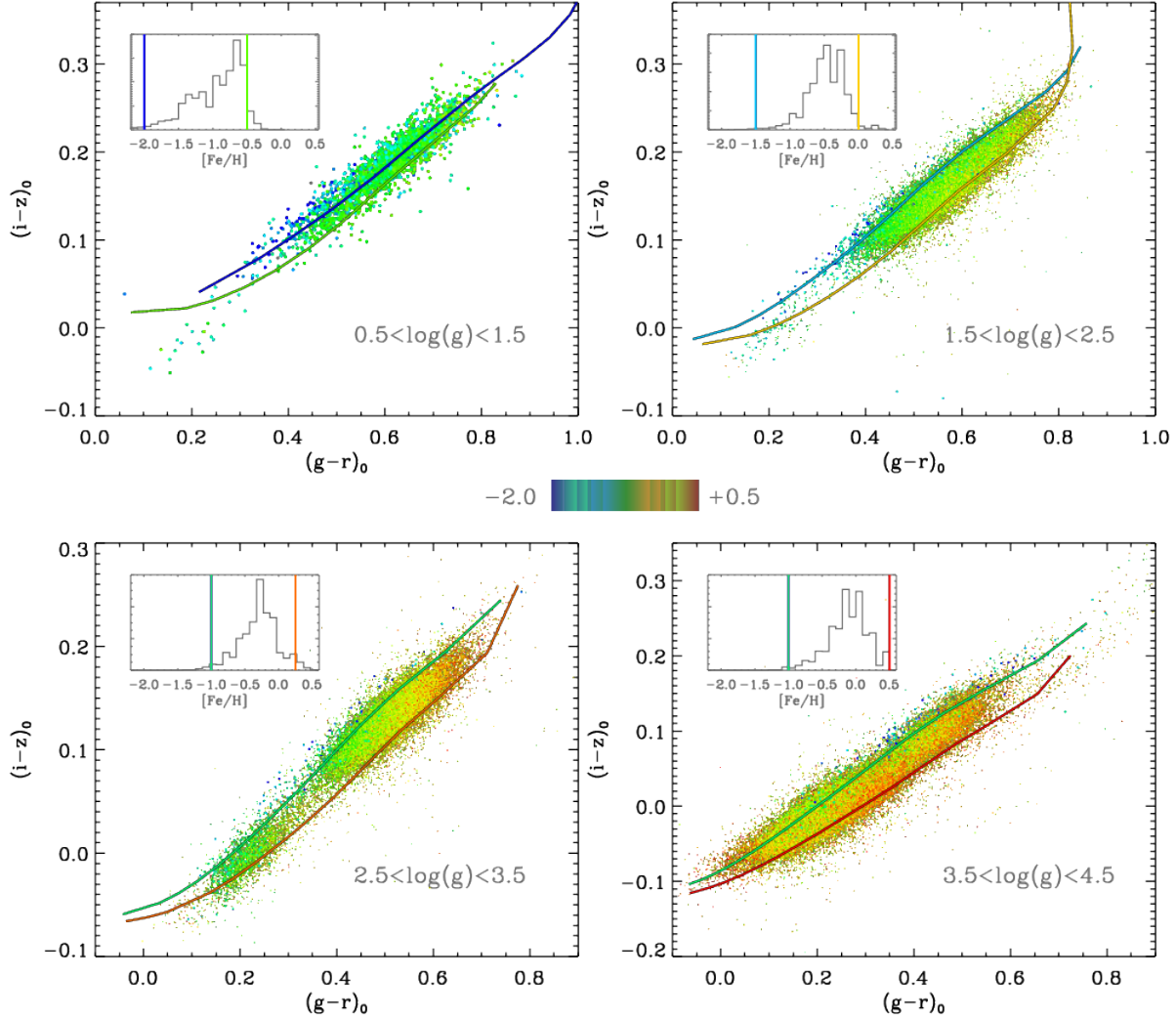


Figure 5. Same as Figure 3 but for a different combination of SkyMapper colours.

4.1.2 Tier 2

Stars in this category still have good stellar parameters, but they lack the full optical and infrared spectrophotometric coverage. They all have STIS observations between 1700 and 10000 Å, a region which encompasses about 70 percent of the bolometric flux, as well as most of the absorption lines in these stars. Longward of 10000 Å the CALSPEC spectrophotometry has been extended with tailored synthetic fluxes (Bohlin 2014; Bohlin et al. 2017). All stars in this category are nearby (~ 25 –75 pc), and hence located within the local bubble where reddening is virtually non-existent (e.g., Leroy 1993; Lallement et al. 2003). The absence of any measurable reddening is confirmed by $H\beta$ photometry (Holmberg et al. 2007). For all of these stars we adopt stellar parameters from the latest revision of the Geneva-Copenhagen Survey (Casagrande et al. 2011).

For stars in this category as well, we usually recover their CALSPEC bolometric fluxes to within ≈ 1 percent in each band, although occasionally the agreement downgrades to approximately 5 percent. Flux uncertainties estimated from MonteCarlo simulations are usually larger than the differences with respect to CALSPEC,

suggesting that the precision at which we recover bolometric fluxes is higher than that inferred from the MonteCarlo analyses.

4.1.3 Tier 3

Finally, we list stars which are affected by reddening as Tier 3. These stars are further away, generally at ~ 100 pc, and they all happen to be metal-poor. In this case, we apply the same reddening corrections to the CALSPEC spectra, as well as to the observed photometry. As for stars in the Tier 2 category, all of these stars have STIS observations between 1700 and 10000 Å, with extensions longward of 10000 Å derived from model atmospheres. We adopt stellar parameters from Meléndez et al. (2010), who determined the reddenings of these stars from interstellar NaID lines. Also, the T_{eff} scale for stars in both Tier 2 (Casagrande et al. 2011) and Tier 3 (Meléndez et al. 2010) is based on the same implementation of the infrared flux method (Casagrande et al. 2010).

We use synthetic photometry of an archetypal metal-poor star ($T_{\text{eff}} = 6000\text{K}$, $\log g = 4.0$, $[\text{Fe}/\text{H}] = -2.0$) to assess the impact of reddening on bolometric flux. A variation of 0.01 in $E(B-V)$ affects

Table 2. CALSPEC bolometric fluxes ($\text{erg s}^{-1} \text{cm}^{-2}$) vs. those recovered interpolating our tables at the given T_{eff} , $\log g$ and $[\text{Fe}/\text{H}]$ in a number of filters. In Eq.(3) we have adopted $L_{\odot} = 3.842 \times 10^{33} \text{erg s}^{-1}$ (Bahcall et al. 2006) which at $R_{\odot} = 6.957 \times 10^{10} \text{cm}$ yields $T_{\text{eff},\odot} = 5777 \text{K}$ consistent with the solar effective temperature in the MARCS library.

Star	Tier	T_{eff} (K)	$\log g$	$[\text{Fe}/\text{H}]$	$E(B - V)$	f_{Bol} CALSPEC	f_{Bol} MARCS	$\sigma(\%)$	$\Delta(\%)$
HD209458	1	6070	4.38	0.00	0	2.289×10^{-8}	$\langle \rangle$: 2.285×10^{-8}		-0.18%
							H_p : 2.259×10^{-8}	1.38	-1.32%
							B_T : 2.257×10^{-8}	1.94	-1.42%
							V_T : 2.296×10^{-8}	1.24	0.32%
							J : 2.330×10^{-8}	2.03	1.81%
							H : 2.303×10^{-8}	3.67	0.60%
							K_S : 2.265×10^{-8}	2.66	-1.05%
HD31128	2	6093	4.46	-1.58	0	6.429×10^{-9}	$\langle \rangle$: 6.427×10^{-9}		-0.02%
							H_p : 6.354×10^{-9}	1.07	-1.16%
							B_T : 6.568×10^{-9}	4.20	2.17%
							V_T : 6.395×10^{-9}	1.80	-0.52%
							J : 6.653×10^{-9}	4.85	3.50%
							H : 6.389×10^{-9}	6.58	-0.61%
							K_S : 6.360×10^{-9}	6.68	-1.07%
							B : 6.227×10^{-9}	3.70	-3.14%
							V : 6.425×10^{-9}	1.60	-0.06%
							R_C : 6.419×10^{-9}	1.72	-0.15%
							I_C : 6.484×10^{-9}	2.64	0.86%
HD106252	2	5903	4.38	-0.06	0	2.903×10^{-8}	$\langle \rangle$: 2.896×10^{-8}		-0.25%
							H_p : 2.845×10^{-8}	0.92	-1.98%
							B_T : 2.843×10^{-8}	3.29	-2.05%
							V_T : 2.878×10^{-8}	1.38	-0.87%
							J : 2.894×10^{-8}	2.93	-0.32%
							H : 2.947×10^{-8}	5.14	1.54%
							K_S : 2.967×10^{-8}	3.79	2.19%
HD159222	2	5786	4.37	0.15	0	6.568×10^{-8}	$\langle \rangle$: 6.574×10^{-8}		0.09%
							H_p : 6.518×10^{-8}	0.89	-0.76%
							B_T : 6.666×10^{-8}	3.07	1.49%
							V_T : 6.550×10^{-8}	1.24	-0.27%
							J : 6.684×10^{-8}	2.50	1.77%
							H : 6.629×10^{-8}	3.35	0.93%
							K_S : 6.568×10^{-8}	2.83	0.00%
							B : 6.532×10^{-8}	2.80	-0.55%
HD185975	2	5671	4.01	0.06	0	1.587×10^{-8}	$\langle \rangle$: 1.574×10^{-8}		-0.77%
							H_p : 1.551×10^{-8}	1.26	-2.26%
							B_T : 1.564×10^{-8}	4.11	-1.43%
							V_T : 1.553×10^{-8}	1.62	-2.16%
							J : 1.598×10^{-8}	2.83	0.68%
							H : 1.586×10^{-8}	3.77	-0.06%
							K_S : 1.596×10^{-8}	4.16	0.58%
HD205905	2	5991	4.49	0.09	0	5.374×10^{-8}	$\langle \rangle$: 5.249×10^{-8}		-2.32%
							H_p : 5.179×10^{-8}	1.34	-3.64%
							B_T : 5.075×10^{-8}	4.75	-5.57%
							V_T : 5.222×10^{-8}	1.60	-2.83%
							J : 5.165×10^{-8}	3.68	-3.90%
							H : 5.463×10^{-8}	5.32	1.65%
							K_S : 5.393×10^{-8}	5.46	0.35%
HD37962	2	5756	4.46	-0.26	0	2.010×10^{-8}	$\langle \rangle$: 1.987×10^{-8}		-1.13%
							H_p : 1.974×10^{-8}	1.19	-1.83%
							B_T : 1.921×10^{-8}	3.94	-4.46%
							V_T : 1.980×10^{-8}	1.59	-1.51%
							J : 1.980×10^{-8}	2.93	-1.51%
							H : 2.041×10^{-8}	4.59	1.53%
							K_S : 2.030×10^{-8}	4.16	0.97%

Table 2. Continued

Star	Tier	T_{eff} (K)	$\log g$	[Fe/H]	$E(B - V)$	f_{Bol} CALSPEC	f_{Bol} MARCS	$\sigma(\%)$	$\Delta(\%)$
HD38949	2	6065	4.47	-0.16	0	2.035×10^{-8}	$\langle \rangle$: 2.002×10^{-8}		-1.66%
							H_P : 1.981×10^{-8}	1.13	-2.69%
							B_T : 1.938×10^{-8}	3.94	-4.76%
							V_T : 1.985×10^{-8}	1.46	-2.46%
							J : 2.030×10^{-8}	3.81	-0.28%
							H : 2.069×10^{-8}	5.26	1.67%
							K_S : 2.006×10^{-8}	4.84	-1.46%
BD+02 3375	3	6163	4.13	-2.24	0.034	3.446×10^{-9}	$\langle \rangle$: 3.386×10^{-9}		-1.75%
							H_P : 3.385×10^{-9}	0.90	-1.76%
							B_T : 3.369×10^{-9}	3.71	-2.25%
							V_T : 3.250×10^{-9}	2.64	-5.69%
							J : 3.498×10^{-9}	3.66	1.52%
							H : 3.431×10^{-9}	6.03	-0.43%
							K_S : 3.328×10^{-9}	5.86	-3.41%
							B : 3.372×10^{-9}	2.96	-2.16%
							V : 3.419×10^{-9}	1.54	-0.79%
							R_C : 3.393×10^{-9}	1.49	-1.52%
							I_C : 3.412×10^{-9}	2.05	-0.98%
BD+21 0607	3	6285	4.29	-1.56	0.020	6.228×10^{-9}	$\langle \rangle$: 6.249×10^{-9}		0.34%
							H_P : 6.145×10^{-9}	0.88	-1.33%
							B_T : 6.514×10^{-9}	3.27	4.59%
							V_T : 6.007×10^{-9}	1.96	-3.55%
							J : 6.354×10^{-9}	3.53	2.02%
							H : 6.261×10^{-9}	4.91	0.53%
							K_S : 6.204×10^{-9}	5.07	-0.39%
							B : 6.244×10^{-9}	2.88	0.25%
							V : 6.290×10^{-9}	1.56	0.99%
							R_C : 6.198×10^{-9}	1.59	-0.48%
							I_C : 6.273×10^{-9}	2.13	0.72%
BD+29 2091	3	5974	4.58	-1.99	0.004	2.363×10^{-9}	$\langle \rangle$: 2.354×10^{-9}		-0.36%
							H_P : 2.324×10^{-9}	0.81	-1.62%
							B_T : 2.294×10^{-9}	5.33	-2.90%
							V_T : 2.226×10^{-9}	4.22	-5.81%
							J : 2.416×10^{-9}	3.66	2.24%
							H : 2.420×10^{-9}	4.66	2.43%
							K_S : 2.405×10^{-9}	5.12	1.77%
							B : 2.350×10^{-9}	3.03	-0.54%
							V : 2.400×10^{-9}	1.50	1.58%
BD+54 1216	3	6127	4.29	-1.63	0.002	3.812×10^{-9}	$\langle \rangle$: 3.816×10^{-9}		0.09%
							H_P : 3.775×10^{-9}	0.89	-0.98%
							B_T : 3.773×10^{-9}	3.61	-1.04%
							V_T : 3.994×10^{-9}	2.29	4.78%
							J : 3.936×10^{-9}	3.73	3.24%
							H : 3.790×10^{-9}	4.76	-0.58%
							K_S : 3.759×10^{-9}	4.94	-1.40%
							B : 3.748×10^{-9}	2.98	-1.67%
							V : 3.801×10^{-9}	1.55	-0.31%
							R_C : 3.797×10^{-9}	1.59	-0.40%
							I_C : 3.783×10^{-9}	2.14	-0.76%
HD74000	3	6362	4.12	-2.01	0.003	4.005×10^{-9}	$\langle \rangle$: 3.965×10^{-9}		-0.99%
							H_P : 3.937×10^{-9}	0.91	-1.68%
							B_T : 3.724×10^{-9}	3.96	-7.00%
							V_T : 3.976×10^{-9}	2.99	-0.72%
							J : 3.896×10^{-9}	4.37	-2.71%
							H : 4.175×10^{-9}	5.42	4.25%
							K_S : 3.983×10^{-9}	5.04	-0.53%
							B : 3.921×10^{-9}	2.89	-2.08%
							V : 4.002×10^{-9}	1.56	-0.07%
							R_C : 3.994×10^{-9}	1.51	-0.26%
							I_C : 4.042×10^{-9}	2.06	0.94%

Table 2. Continued

Star	Tier	T_{eff} (K)	$\log g$	[Fe/H]	$E(B - V)$	f_{Bol} CALSPEC	f_{Bol} MARCS	$\sigma(\%)$	$\Delta(\%)$
HD160617	3	6048	3.73	-1.78	0.005	9.510×10^{-9}	$\langle \rangle: 9.406 \times 10^{-9}$		-1.09%
							$H_P: 9.482 \times 10^{-9}$	1.14	-0.30%
							$B_T: 9.520 \times 10^{-9}$	3.62	0.11%
							$V_T: 9.286 \times 10^{-9}$	2.00	-2.35%
							$J: 9.582 \times 10^{-9}$	3.62	0.75%
							$H: 9.390 \times 10^{-9}$	5.65	-1.27%
							$K_S: 9.261 \times 10^{-9}$	5.27	-2.62%
							$B: 9.390 \times 10^{-9}$	3.29	-1.27%
							$V: 9.390 \times 10^{-9}$	1.66	-1.27%
							$R_C: 9.372 \times 10^{-9}$	1.50	-1.45%
							$I_C: 9.390 \times 10^{-9}$	2.02	-1.27%

f_{Bol} MARCS is the bolometric flux recovered in different bands: H_P Hipparcos, $B_T V_T$ Tycho, JHK_S 2MASS and $BV(RI)_C$ Johnson-Cousins. For the latter system we have used the *ubvri12* transformations (see Paper I). $\langle \rangle$ is the average of all systems listed for a given star. $\sigma(\%)$ is the percent uncertainty in the bolometric flux recovered from a single band, and estimated from MonteCarlo as described in text. $\Delta(\%)$ is the percent difference between the CALSPEC bolometric flux and that recovered from our bolometric corrections. In case of reddening, also the CALSPEC flux has been corrected by the same amount, with the same extinction law adopted in our tables of bolometric corrections.

the recovered bolometric flux by an amount which varies between 0.3–0.8 percent in the infrared, to around 2–3 percent in the optical. On average we recover the CALSPEC bolometric fluxes to within ≈ 1 percent, but single bands can occasionally return differences as large as 5–7 percent. Also in this case, differences with respect to CALSPEC bolometric fluxes are usually within the MonteCarlo uncertainties.

4.1.4 Regarding the precision and accuracy of bolometric fluxes

In the above comparisons, we have estimated the mean uncertainty in recovering bolometric fluxes using MonteCarlo studies that take into account the uncertainties in the input parameters and observed photometry. The mean uncertainty in the bolometric fluxes obtained from our tables increases from around 2 percent for the star in Tier 1, to 3 percent for stars in Tier 3, reflecting the lower quality of the input parameters. However, comparisons with CALSPEC fluxes suggest that the precision is usually better than those derived from the MonteCarlo analyses.

For a given band, the average difference between the fluxes we recover and the CALSPEC observations is ± 1.1 percent at Tier 1, increasing to ± 1.7 percent and ± 1.8 percent for stars in the Tier 2 and Tier 3 categories, respectively. When combining the results for all available bands, the mean difference varies from -0.2 percent for the Tier 1 star, to ~ -0.7 percent for stars in the Tier 2 and 3 categories. This difference is clearly systematic, in the sense that our fluxes are usually smaller. These findings could be modified by changing the adopted value of L_\odot , but it should also be kept in mind that the systematic uncertainty in CALSPEC spectrophotometry is at the 1 percent level (Bohlin 2014). Hence, we conclude that, when combining the results from different bands, it is feasible to recover the bolometric flux to within 1 percent, below which we are limited by the fundamental uncertainty of the current absolute flux scale.

4.2 Testing colour indices

Another way to test the performance of our synthetic photometry is by comparing various combinations of synthetic and observed colours for stars of known stellar parameters. In order to do this, we cross-matched RAVE DR5 (Kunder et al. 2017) with the Tycho, 2MASS and SkyMapper catalogues. RAVE DR5 provides stellar

parameters for nearly 0.5 million stars in the southern hemisphere: we retained only those stars with the best determined stellar parameters (`ALGO_CONV=0`, `c1=c2=c3=n`). We rescaled the reddening from Schlegel et al. (1998) as described in Kunder et al. (2017, which in fact provides overall good agreement between photometric and spectroscopic T_{eff}). In addition, to avoid regions with severe extinction, we considered only stars at Galactic latitudes $|b| > 10^\circ$ and excluded stars with rescaled $E(B - V) \geq 0.1$. Further cuts on photometric quality were also applied, depending on the filters (see captions to figures), typically yielding $> 100,000$ usable stars. We compared observed and synthetic colours by plotting stars in different ranges of $\log g$. Stars with lower surface gravities have higher intrinsic luminosities, and thus in RAVE (grossly magnitude limited) they span larger distances. The metallicity gradients in the Galactic disc (e.g., Boeche et al. 2013, 2014) explain why the bulk metallicity decreases with decreasing $\log g$.

MARCS synthetic colours perform overall well across a wide range of filters and stellar parameters, as showcased in Figure 2 through 5. They are able to predict the main observed features, although they fail in the $u - g$ vs $g - r$ plane at the lowest gravities and hottest T_{eff} . To better quantify these findings, we generated synthetic colours for each RAVE DR5 star that passed our quality and photometric cuts. This is shown in Figure 6, which compares observed and synthetic colours as function of stellar parameters. Again, the overall agreement between observed and synthetic photometry is quite remarkable, with mean offsets that are always within the scatter and never exceeding a few hundredths of a mag. In particular, the Tycho and 2MASS colours have nearly no offsets, indicating that the synthetic colours in these two systems are extremely well standardised (both observationally and theoretically). The overall agreement for the SkyMapper colours is equally remarkable, especially considering that, at the present time, the exact standardisation of observed SkyMapper photometry to the AB system is still work in progress.

It can immediately be seen that indices involving bluer colours ($B_T - V_T$ and $u - g$), while well centred at the solar [Fe/H], are increasingly offset at higher and lower metallicities. This is likely due to the fact that, at short wavelengths, synthetic spectra depend critically on the adopted opacities and microturbulence (see the discussion in Paper I). The SkyMapper u filter is also sensitive to gravity, and it is apparent the predicted colours depart from the observed ones for $\log g < 1.5$. There is also a tendency for the synthetic

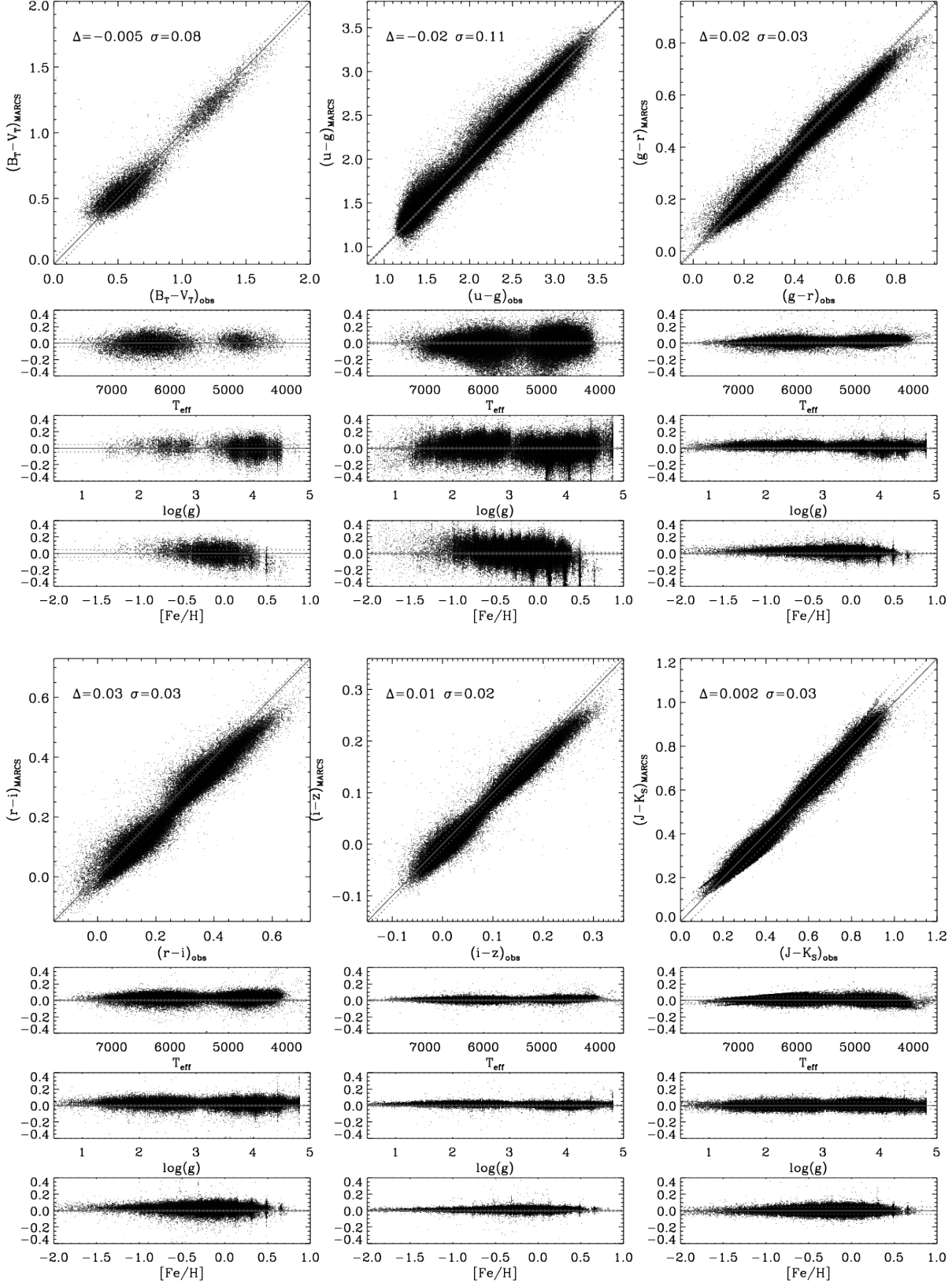


Figure 6. Comparison between observed and synthetic MARCS colours interpolated from our tables at the IRFM T_{eff} , $\log g$, $[\text{Fe}/\text{H}]$ and rescaled $E(B - V)$ of each RAVE DR5 star. Continuous gray line is the one-to-one relation, whereas dotted lines indicate the mean scatter arising solely from observed photometric errors. Δ and σ are the mean colour index difference (observed minus synthetic) and scatter in mag.

colours to be bluer than observed at $T_{\text{eff}} \lesssim 4500$ K, which could indicate missing molecular opacities.

4.3 Star Cluster Colour-Magnitude Diagrams

The colour-magnitude diagrams (CMDs) of open and globular star clusters provide especially good constraints on properties of stellar models for lower mass stars, including their colours, because the member stars have very close to the same age and initial chemical abundances (modulo the presence of multiple populations, see e.g., Gratton et al. 2012, for a review). The CMDs therefore describe how the colours (and effective temperatures) of stars vary with gravity at a fixed age and metallicity. Even though current stellar models appear to be able to reproduce the principal photometric sequences of star clusters quite well (see, e.g., VandenBerg et al. 2013, VandenBerg et al. 2014; Paper I), the predicted T_{eff} scale is subject to uncertainties associated with, e.g., convection theory, the atmospheric boundary condition, and the treatment of diffusive processes, while synthetic colours depend sensitively on T_{eff} , the temperature structures of model atmospheres, the treatment of blanketing, etc. Consequently, one should not expect to find perfect agreement between isochrones that have been transformed to various observational planes and observed CMDs.

Still, the consistency of predicted colour- T_{eff} relations can be tested by determining if the same interpretation of the data (including discrepancies between theory and observations) is found on many different CMDs. For instance, in the study of $UBV(RI)_C$, Sloan ($ugriz$), and HST -ACS photometry of the globular cluster (GC) M5 that was presented in Paper I (see their figs. 9–11), the red giant branch (RGB) of the isochrone that was fitted to the observations was consistently located along the red edge of the observed distribution of giants in all of the different CMDs that were considered. The most likely explanation of this offset is that the predicted temperatures along the RGB are somewhat too cool. Moreover, with the exception of the $[(F606W - F814W), F606W]$ - and $[(g - r), r]$ -diagrams, the same isochrone provided an excellent match to the turnoff (TO) and upper main sequence (MS) observations. Here again, very encouraging consistency was found, though it would appear that either the HST and Sloan observations (in the $F606W$ and/or the $F814W$ passbands and in the g and/or r filters, respectively), or the corresponding bolometric correction transformations presented in Paper I, suffer from small zero-point errors.

This investigation affords us with the opportunity to extend the aforementioned analysis of star cluster CMDs to the Pan-STARRS1 photometric system given that Bernard et al. (2014) have published well-defined fiducial sequences for the same GC (M5) and open clusters (M67 and NGC 6791) that were considered in Paper I. If, as adopted previously, an isochrone for 11.75 Gyr, $[\text{Fe}/\text{H}] = -1.33$, $[\alpha/\text{Fe}] = 0.4$, and $Y = 0.25$ is overlaid onto the Pan-STARRS1 fiducials assuming the same cluster parameters ($E(B - V) = 0.032$ and a true distance modulus $(m - M)_0 = 14.35$), we obtain the results shown in Figure 7. As before, the observed RGB is somewhat bluer than the predicted giant branch, though both loci have nearly the same slope, while the upper MS observations are generally quite well matched by the models — except in the case of the $[(g - r), g]$ -diagram, where the isochrone is too blue by ~ 0.02 mag. Since no such problem is apparent in the other CMDs that involve the g passband, it would appear that there is a small zero-point problem with either the r photometry or the BC_r predictions. Nevertheless, for the most part, the selected isochrone provides nearly identical fits to Pan-STARRS1 observations as to $BV(RI)_C$ and Sloan data (see

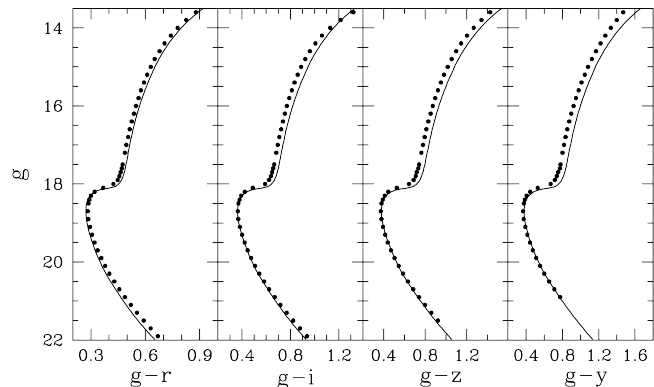


Figure 7. Overlay of an 11.75 Gyr isochrone for $[\text{Fe}/\text{H}] = -1.33$, $[\alpha/\text{Fe}] = 0.4$, and $Y = 0.25$ (solid curve) to the principal photometric sequences of M5 (small filled circles) that were derived by Bernard et al. (2014) from their Pan-STARRS1 *grizy* observations. The transformation of the isochrone to the observed planes assumes $E(B - V) = 0.032$ (e.g., Schlafly & Finkbeiner 2011) and $(m - M)_0 = 14.35$.

Paper I). This indicates that the transformations to the different photometric systems are highly consistent with one another.

The fact that bluer colours are more difficult to match than those derived from filters at longer wavelengths is almost certainly due primarily to deficiencies in the modelling of stellar atmospheres and synthetic spectra, as is the increased difficulty of explaining the colours of cooler stars. For instance, figure 14 in Paper I shows that a 4.3 Gyr, solar abundance isochrone provides a very good fit to the MS of the open cluster M67 down to $V \sim 16.7$ on the $[(B - V), V]$ -diagram, as compared with $V \sim 19$ on the $[(V - K_s), V]$ -diagram. Moreover, at fainter magnitudes, the differences between the predicted and observed colours typically increase with decreasing T_{eff} . The same behaviour is found (see Figure 8) when the same isochrone is fitted to Pan-STARRS1 photometry of M67 (Bernard et al. 2014) on the assumption of $E(B - V) = 0.03$ and $(m - M)_0 = 9.60$ (as adopted in Paper I). On the one hand, it is very gratifying to find that this isochrone provides a superb fit to the upper MS, irrespective of the filter system that was employed. On the other hand, it is clear that the predicted colours of lower-MS stars are too blue by $\gtrsim 0.2$ mag at $g > 20$. (We note that such CMD comparisons as those plotted in Figure 8 could be used to derive empirical corrections to the purely synthetic colours.)

Although an isochrone for 8.5 Gyr, $[\text{Fe}/\text{H}] = +0.30$, $[\alpha/\text{Fe}] = 0.0$, and $Y = 0.28$ provides a very good fit, in an absolute sense, to many of the CMDs of NGC 6791 that can be constructed from BVI_CJ and Sloan *ugriz* photometry (see figures 12 and 13 in Paper I), it does not reproduce the fiducial sequences that were derived from Pan-STARRS1 observations by Bernard et al. (2014) quite as well. As shown in Figure 9, the predicted TO and RGB tend to be somewhat too red if $E(B - V) = 0.16$ and $(m - M)_0 = 13.05$ (as adopted in Paper I, which discusses recent determinations of the cluster parameters), whereas no such discrepancies were found previously. Much better consistency can be obtained if $E(B - V) = 0.14$ (the red curve) or a slightly larger value, likely indicating a small zero-point offset (0.01 – 0.02 mag) between Pan-STARRS1 photometry and Johnson-Cousins-Sloan observations of NGC 6791. In fact, a small difference in the same sense was found by Bernard et al. (2014, see their figure 5) when they compared their fiducial sequences with those obtained by transforming the Sloan CMDs

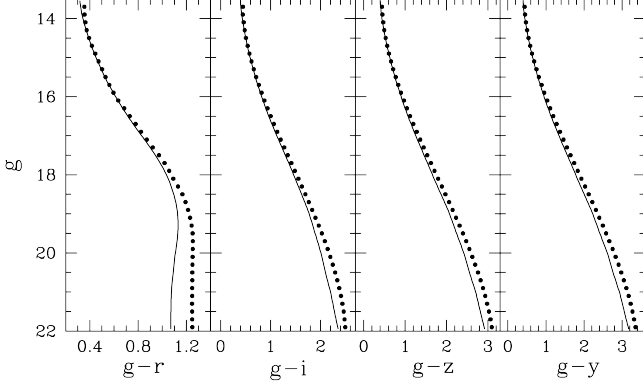


Figure 8. Similar to the previous figure; in this case, a 4.3 Gyr isochrone for $[\text{Fe}/\text{H}] = 0.0$ and $Y = 0.255$ has been overlaid on the main-sequence fiducial of M67 derived by Bernard et al. (2014), assuming $E(B - V) = 0.03$ (e.g., Schlafly & Finkbeiner 2011) and $(m - M)_0 = 9.60$.

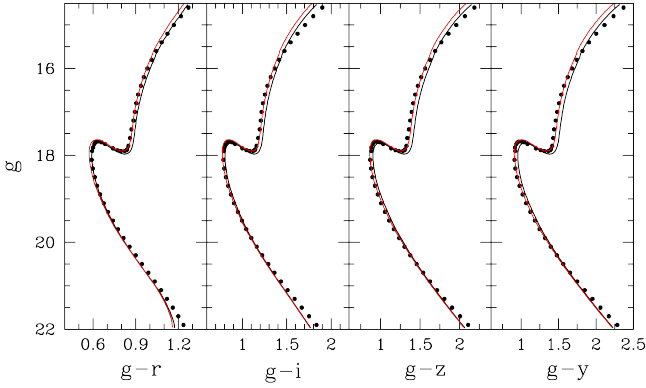


Figure 9. Similar to the previous two figures; in this case, an isochrone for 8.5 Gyr, $[\text{Fe}/\text{H}] = +0.30$, and $Y = 0.28$ has been overlaid on the main-sequence fiducial of NGC 6791 derived by Bernard et al. (2014), assuming $(m - M)_0 = 13.05$ and $E(B - V) = 0.16$ (black curve) or 0.14 (red curve).

given by An et al. (2008) to the Pan-STARRS1 system. Although further work is needed to fully understand this discrepancy, this level of consistency is still quite satisfactory given that observations typically involve zero-point uncertainties close to 0.01 mag (see e.g., Stetson 2005).

In fact, it is remarkable that the Pan-STARRS1 transformations yield colours that provide fully consistent interpretations of the data (to within 0.01 mag) as the transformations considered in Paper I over a wide range in metallicity and gravity — especially for stars within $\sim \pm 2$ mag of the turnoff.

5 CONCLUSIONS

In this paper we have continued our effort to provide reliable and well tested synthetic colours and bolometric corrections from the MARCS library for various combinations of T_{eff} , $\log g$, $[\text{Fe}/\text{H}]$ and $[\alpha/\text{Fe}]$. We have extended our previous investigation (Paper I) to include many of the systems underpinning large photometric surveys in the optical (Hipparcos/Tycho, Pan-STARRS1 and SkyMapper), and we plan to add *Gaia* photometry once the transmission curves and standardisation details become available. Together with 2MASS and SDSS (included in Paper I, among other systems),

these surveys are fostering a wide variety of studies in stellar and Galactic astronomy. However to reap the maximum returns, properly standardised, reliable and well tested stellar synthetic colours are needed to interpret the observations.

Encouragingly, our study of star clusters has demonstrated that isochrones generally provide very similar fits to observed CMDs in different photometric systems under the same assumptions concerning the age, reddening and distance modulus. Small adjustments at the level of 0.01 – 0.02 mag are sometimes needed to obtain fully consistent interpretations of the data, but this appears to be an exception more than the rule. This indicates that overall we have achieved our goal of providing synthetic colours that are homogeneously standardised across different system to within ~ 0.01 mag, which is also the zero-point limit of typical ground-based observations.

Once we trust our zero-points, we can have meaningful discussions concerning the performance of the MARCS synthetic photometry. We have done so by computing synthetic colours for more than a hundred thousand stars from RAVE DR5, and comparing them with the observed colours. Overall, we find very satisfactory agreement of optical and infrared colours for most of the parameter space that has been explored. However, at short wavelengths, models have some difficulties predicting colours for stars with gravities roughly below $\log g = 1.5$, and while good agreement between observed and synthetic colours is always found close to the solar metallicity, differences become evident in the direction of both lower and higher $[\text{Fe}/\text{H}]$. Irrespective of the filters that are used, discrepancies always begin to appear as the temperature drops toward the coolest T_{eff} values that we have considered. We recall from Paper I that for the blue and ultraviolet spectral region (in particular for the coolest and most metal rich stars) synthetic colours show dependence on microturbulence, which is fixed to 2 km s^{-1} in this investigation. (Note that this investigation has focused on FGK type stars. Although we predict the BCs for M dwarfs and giants, their performance is not as thoroughly tested as for earlier spectral types.)

HST spectrophotometry has enabled us to perform the most stringent test yet on the level at which bolometric fluxes can be recovered from our tables of synthetic BCs. For FG dwarfs of known input stellar parameters, we conclude that, on average, bolometric fluxes can be recovered to within about 2 percent from our computed bolometric corrections in a single band, and that this uncertainty is usually halved when combining the results from more bands. To facilitate further investigations of MARCS colours, we have provided tables of BCs and suitable computer programs to interpolate in them for any combination of T_{eff} , $\log g$, $[\text{Fe}/\text{H}]$ and $[\alpha/\text{Fe}]$ that is contained within the MARCS library. The most obvious application of these data and interpolation codes, which are described in the Appendix, is to transpose isochrones to many different CMDs. Among the photometric systems that have been considered (here and in Paper I), we have included synthetic photometry for the imaging cameras on *JWST*. While the standardisation of real data from *JWST* may turn out to be somewhat different from what we have assumed, our programs make it possible to obtain a first estimate of the appearance of stellar populations through the eye of *JWST* and, therefore, to assist with the planning of future observations.

ACKNOWLEDGMENTS

LC gratefully acknowledges support from the Australian Research Council (grants DP150100250, FT160100402), while the contributions of D.A.V to this project were supported by a Discovery Grant from the Natural Sciences and Engineering Research Council of Canada. We thank Andrea Kunder for useful advice on the use of RAVE flags, Edouard Bernard for providing machine-readable versions of the globular cluster fiducials in Pan-STARRS1, George Rieke for helpful correspondence on JWST filters, and Mike Bessell for comments. The national facility capability for SkyMapper has been funded through ARC LIEF grant LE130100104 from the Australian Research Council, awarded to the University of Sydney, the Australian National University, Swinburne University of Technology, the University of Queensland, the University of Western Australia, the University of Melbourne, Curtin University of Technology, Monash University and the Australian Astronomical Observatory. SkyMapper is owned and operated by The Australian National University's Research School of Astronomy and Astrophysics. The survey data were processed and provided by the SkyMapper Team at ANU. The SkyMapper node of the All-Sky Virtual Observatory (ASVO) is hosted at the National Computational Infrastructure (NCI). Development and support the SkyMapper node of the ASVO has been funded in part by Astronomy Australia Limited (AAL) and the Australian Government through the Commonwealth's Education Investment Fund (EIF) and National Collaborative Research Infrastructure Strategy (NCRIS), particularly the National eResearch Collaboration Tools and Resources (NeCTAR) and the Australian National Data Service Projects (ANDS). This publication makes use of data products from the Two Micron All Sky Survey, which is a joint project of the University of Massachusetts and the Infrared Processing and Analysis Center/California Institute of Technology, funded by the National Aeronautics and Space Administration and the National Science Foundation. Funding for RAVE (www.rave-survey.org) has been provided by institutions of the RAVE participants and by their national funding agencies.

REFERENCES

- An D. et al., 2008, *ApJS*, 179, 326
 Asplund M., Grevesse N., Sauval A. J., Scott P., 2009, *ARA&A*, 47, 481
 Bahcall J. N., Serenelli A. M., Basu S., 2006, *ApJS*, 165, 400
 Bernard E. J. et al., 2014, *MNRAS*, 442, 2999
 Bessell M., Murphy S., 2012, *PASP*, 124, 140
 Bessell M., Bloxham G., Schmidt B., Keller S., Tisserand P., Francis P., 2011, *PASP*, 123, 789
 Bessell M. S., 2000, *PASP*, 112, 961
 Boeche C. et al., 2013, *A&A*, 559, A59
 Boeche C. et al., 2014, *A&A*, 568, A71
 Bohlin R. C., 2014, *AJ*, 147, 127
 Bohlin R. C., Mészáros S., Fleming S. W., Gordon K. D., Koeke-moer A. M., Kovács J., 2017, *AJ*, 153, 234
 Bonifacio P. et al., 2018, *A&A*, in press
 Cardelli J. A., Clayton G. C., Mathis J. S., 1989, *ApJ*, 345, 245
 Casagrande L., VandenBerg D. A., 2014, *MNRAS*, 444, 392
 Casagrande L., Ramírez I., Meléndez J., Bessell M., Asplund M., 2010, *A&A*, 512, A54+
 Casagrande L., Schönrich R., Asplund M., Cassisi S., Ramírez I., Meléndez J., Bensby T., Feltzing S., 2011, *A&A*, 530, A138
 Chambers K. C. et al., 2016, *ArXiv e-prints*
 Chiavassa A., Casagrande L., Collet R., Magic Z., Bigot L., Thevenin F., Asplund M., 2018, *A&A*, in press
 del Burgo C., Allende Prieto C., 2016, *MNRAS*, 463, 1400
 Fritz T. K. et al., 2011, *ApJ*, 737, 73
 Fukugita M., Ichikawa T., Gunn J. E., Doi M., Shimasaku K., Schneider D. P., 1996, *AJ*, 111, 1748
 Gaia Collaboration et al., 2016, *A&A*, 595, A1
 Gardner J. P. et al., 2006, *Space Sci. Rev.*, 123, 485
 Gordon K., Bohlin R., Fullerton A., Beck T., Robberto M., 2009, *JWST-STScI-001855*
 Gratton R. G., Carretta E., Bragaglia A., 2012, *A&A Rev.*, 20, 50
 Gustafsson B., Edvardsson B., Eriksson K., Jørgensen U. G., Nordlund Å., Plez B., 2008, *A&A*, 486, 951
 Hanbury Brown R., Davis J., Allen L. R., Rome J. M., 1967, *MNRAS*, 137, 393
 Høg E. et al., 2000, *A&A*, 355, L27
 Holmberg J., Nordström B., Andersen J., 2007, *A&A*, 475, 519
 Karovicova I. et al., 2018, *ArXiv e-prints*
 Kunder A. et al., 2017, *AJ*, 153, 75
 Lallement R., Welsh B. Y., Vergely J. L., Crifo F., Sfeir D., 2003, *A&A*, 411, 447
 Leroy J. L., 1993, *A&A*, 274, 203
 Lindegren L. et al., 2016, *A&A*, 595, A4
 Meléndez J., Casagrande L., Ramírez I., Asplund M., Schuster W. J., 2010, *A&A*, 515, L3+
 Michalik D., Lindegren L., Hobbs D., 2015, *A&A*, 574, A115
 Perryman M. A. C. et al., 1997, *A&A*, 323, L49
 Rieke G. H. et al., 2015, *PASP*, 127, 584
 Rieke M. J., Kelly D., Horner S., 2005, in J.B. Heaney, L.G. Burriesci, eds, *Cryogenic Optical Systems and Instruments XI. Proc. SPIE*, Vol. 5904, pp. 1–8
 Ruchti G. R., Bergemann M., Serenelli A., Casagrande L., Lind K., 2013, *MNRAS*, 429, 126
 Schlafly E. F., Finkbeiner D. P., 2011, *ApJ*, 737, 103
 Schlegel D. J., Finkbeiner D. P., Davis M., 1998, *ApJ*, 500, 525
 Skrutskie M. F. et al., 2006, *AJ*, 131, 1163
 Stetson P. B., 2005, *PASP*, 117, 563
 Tonry J. L. et al., 2012, *ApJ*, 750, 99
 van Leeuwen F., Evans D. W., Grenon M., Grossmann V., Mignard F., Perryman M. A. C., 1997, *A&A*, 323, L61
 VandenBerg D. A., Brogaard K., Leaman R., Casagrande L., 2013, *ApJ*, 775, 134
 VandenBerg D. A., Bergbusch P. A., Ferguson J. W., Edvardsson B., 2014, *ApJ*, 794, 72
 Wolf C. et al., 2018, *PASA*, submitted

APPENDIX A: INTERPOLATION ROUTINES

The Appendix in Paper I provides a detailed and quite thorough description of the library of bolometric corrections (BCs) that has been developed for several of the most widely used broad-band photometric systems (Johnson-Cousins, SDSS, 2MASS, and *HST*-ACS, *HST*-WFC3, calibrated to AB, ST, and VEGA zero-points). It contains data for more than 40 filters, derived from MARCS model atmospheres (Gustafsson et al. 2008, same as used here) that encompass wide ranges in gravity ($-0.5 \leq \log g \leq 5.5$), effective temperature ($2600 \leq T_{\text{eff}} \leq 8000$ K), iron abundance ($-4.0 \leq [\text{Fe}/\text{H}] \leq +1.0$), and α -element abundances ($-0.4 \leq [\alpha/\text{Fe}] \leq +0.4$) — though the coverage is not complete (e.g., BCs are not available for the full range in T_{eff} at all gravities; see figure A2 in Paper I) and the range in $[\text{Fe}/\text{H}]$ varies somewhat for different values of $[\alpha/\text{Fe}]$ (see below). Moreover, BCs have been generated for $E(B - V) = 0.0, 0.12, 0.24, \dots, 0.72$ so that, by interpolation in these results, one can take the effects of interstellar reddening into account. This library is contained in the file `BCTables.tar.gz`, whereas `BCcodes.tar` contains FORTRAN interpolation routines.

In this investigation, we have created a second library (`BCTables2.tar.gz`) comprised of analogous transformations for the SkyMapper, Hipparcos/Tycho, Pan-STARRS1, and *JWST*-NIRCam/MIRI systems. `BCTables2.tar.gz`, together with `BCTables.tar.gz` from Paper I can be use with the new and updated set of interpolation routines described below (`BCcodes.tar`), which supersede those provided in Paper I⁴. Because most users will be interested in only a small subset of the predicted BCs, the supplied FORTRAN codes will generate tables of reddening-corrected BCs, assuming just one user-selected value of $E(B - V)$, for up to a maximum of 5 different filters. The filter selection is controlled by `selectbc.data`, which has already been described in considerable detail in Paper I. In fact, the only substantive change that has been made to this file is an extension of the menu options to include the additional photometric systems and associated filters that are the subject of this paper.

As shown in Figure A1, there are now 22 photometric systems (or variations thereof) and a total of 85 different filters in the combined library. (Because the part of the menu concerning the first seven photometric systems already been discussed in Paper I, it has not been reproduced here.) According to the text below the dashed line, we see, for instance, that the integers 8, 9, and 10 in the left-hand column identify synthetic *JWST*-MIRI photometry, calibrated, in turn, to the AB, ST, and VEGA systems. The only filters that are relevant to these cases are F560W to F1500W, which have integer identifications ranging from 42 to 47, respectively. Similarly, BCs have been computed for 22 *JWST*-NIRCam filters (F070W, F090W, ..., F480M) using module A (`moda`), module B (`modb`), and the average of the two, AB (`modab`). See discussion in Section 2.4.1). Since each of these 3 cases has also been calibrated to the AB, ST, and VEGA systems, NIRCam data has been subdivided into the 9 possibilities that are identified by the integers 11 to 19 in the left-hand column.

Thus, to obtain any BC tables of interest, it is simply a matter of specifying the number of filters (`nfil`) on the second line of `selectbc.data`, followed by pairs of integers on successive lines to identify those filters. In the example given in Figure A1, `nfil = 4` and the selected filters are MIRI F560W, F1280W (calibrated to VEGA zero-points) and Pan-STARRS1 g, i . The first line of

```

1 = ialf (= [alpha/Fe] variation: select from choices listed below)
4 = nfil (= number of filter bandpasses to be considered; maximum = 5)
10 42 = photometric system and filter (select from menu below)
10 46 = photometric system and filter (select from menu below)
22 79 = photometric system and filter (select from menu below)
22 81 = photometric system and filter (select from menu below)
1 3 = photometric system and filter (select from menu below)
-----
ialf: 1: "standard variation" of [alpha/Fe] with [Fe/H] --> bc_std.data
      2: [alpha/Fe] = +0.4 ([Fe/H] from -2.5 to +0.5) --> bc_p04.data
      3: [alpha/Fe] = +0.0 ([Fe/H] from -2.5 to +1.0) --> bc_p00.data
      4: [alpha/Fe] = -0.4 ([Fe/H] from -2.0 to +1.0) --> bc_m04.data

Photometric system <----- Filters ----->

(See Paper I for the first seven photometric systems and associated filters.)

8 = jwst_miri_ab      42 = miri_f560w      43 = miri_f770w      44 = miri_f1000w
9 = jwst_miri_st      45 = miri_f1130w     46 = miri_f1280w     47 = miri_f1500w
10 = jwst_miri_vega

11 = jwst_moda_ab     48 = jwst_f070w      49 = jwst_f090w      50 = jwst_f115w
12 = jwst_moda_st     51 = jwst_f140m      52 = jwst_f150w2     53 = jwst_f150w
13 = jwst_moda_vega   54 = jwst_f162m      55 = jwst_f182m      56 = jwst_f200w
14 = jwst_modab_ab    57 = jwst_f210m      58 = jwst_f250m      59 = jwst_f277w
15 = jwst_modab_st    60 = jwst_f300m      61 = jwst_f322w2     62 = jwst_f335m
16 = jwst_modab_vega  63 = jwst_f356w      64 = jwst_f360m      65 = jwst_f410m
17 = jwst_modb_ab     66 = jwst_f430m      67 = jwst_f444w      68 = jwst_f460m
18 = jwst_modb_st     69 = jwst_f480m

20 = SkyMapper        70 = u               71 = v               72 = g
                       73 = r               74 = i               75 = z

21 = Tycho             76 = Hp              77 = B_T             78 = V_T

22 = PanSTARRS1        79 = g               80 = r               81 = i
                       82 = z               83 = y               84 = w
                       85 = o

```

Figure A1. Listing of the parts of `selectbc.data` relevant to the photometric systems and associated filters considered in this study. (The menu options relevant to the photometric systems considered in Paper I have been omitted, but see figure A3 in that study.) Depending on the values of the integer parameters in the seven lines just above the dashed line, the supplied FORTRAN codes will produce BC tables for up to 5 filters of interest and one of four possible variations of $[\alpha/\text{Fe}]$ with $[\text{Fe}/\text{H}]$ (see the text for a detailed explanation.)

`selectbc.data` contains the parameter `ialf`, which determines whether the BCs are to assume the “standard variation” of $[\alpha/\text{Fe}]$ with $[\text{Fe}/\text{H}]$ (`ialf = 1`), or $[\alpha/\text{Fe}] = +0.4, 0.0$, or -0.4 for the ranges in $[\text{Fe}/\text{H}]$ that are given in the menu (`ialf = 2, 3`, or `4`, respectively). The standard variation assumes that $[\alpha/\text{Fe}] = +0.4$ for $-4.0 \leq [\text{Fe}/\text{H}] < -1.0$, $[\alpha/\text{Fe}] = -0.4 \times [\text{Fe}/\text{H}]$ for $-1.0 \leq [\text{Fe}/\text{H}] \leq 0.0$ (i.e., a linear decrease in $[\alpha/\text{Fe}]$ from $+0.4$ at $[\text{Fe}/\text{H}] = -1.0$ to 0.0 at $[\text{Fe}/\text{H}] = 0.0$), and $[\alpha/\text{Fe}] = 0.0$ for $0.0 \leq [\text{Fe}/\text{H}] \leq +1.0$.

The procedure to compute BCs for different variations of $[\alpha/\text{Fe}]$ was somewhat cumbersome in Paper I. We now provide a new program named `get4bctables.for` to generate BCs tables for the user-selected filters, and all values of `ialf` in a single execution (i.e., the value of `ialf` that is read from `selectbc.data` is ignored at this stage). Figure A2 shows how easy it is to generate the BC tables in the case where `selectbc.data` have the values given in the first seven lines of Figure A1. For the sake of this example, once `get4bctables.for` has been compiled, and the executable module has been named `get4bctables`, one simply has to enter `get4bctables` (on a Linux-like environment this holds true if the executable is placed on the `$PATH`. Otherwise, all executables discussed in this Appendix can be called from the directory they are located in by adding `./` to their names e.g., `./get4bctables`). This will generate a request for the $E(B - V)$ value of interest, to which we have responded with a value of 0.035 (from the permitted

⁴ All material is freely available online through CDS, and kept up-to-date on GitHub github.com/casaluka/bolometric-corrections

```

>get4bctables
  enter E(B-V) value for which BCs are to be generated
> 0.035
files inputbc_r00.data, inputbc_r12.data, etc., have been created for
  MIRIvega: miri_f560w
  MIRIvega: miri_f1280w
  PanSTARR: PanS_g
  PanSTARR: PanS_i

bc_std.data has been created assuming E(B-V) = 0.035

bc_p04.data has been created assuming E(B-V) = 0.035

bc_p00.data has been created assuming E(B-V) = 0.035

bc_m04.data has been created assuming E(B-V) = 0.035

```

Figure A2. Sample execution of `get4bctables`. When the name of this executable module is entered at the prompt (>), the code notifies both the filters selected by the user and the four data files that have been generated containing the reddening-corrected BC tables for those filters.

range $0.0 \leq E(B - V) \leq 0.72$). The code then proceeds to retrieve from the library the data for the selected filters (which are printed on the monitor for the convenience of the user) and to generate `bc_std.data`, `bc_p04.data`, `bc_p00.data`, and `bc_m04.data` for the specified reddening. These `bc_***.data` files can then be used e.g., to compute bolometric corrections (and colour indices) of stars of known T_{eff} , $\log g$ and $[\text{Fe}/\text{H}]$, at the reddening entered above. This can be done using the program `bcstars.for` (which will call subroutines contained in `bcutil.for` for the appropriate value of `ialf`).

The above procedure (editing `selectbc.data`, executing `get4bctables`, and `bcstars`) is easily repeated to obtain the BCs for a different reddening and/or an alternative selection of filters and/or a different list of input stellar parameters. Importantly, our programs assume a certain directory structure to be in place. Hence, the libraries in `BCTables.tar.gz` and `BCTables2.tar.gz` *must* be unpacked in the same directory as the various FORTRAN codes and `selectbc.data`.

As described above, our routines can be used to compute bolometric corrections at given input of T_{eff} , $\log g$ and $[\text{Fe}/\text{H}]$ for selected values of $[\alpha/\text{Fe}]$. These inputs can be e.g., from a sample of stars; from a list covering a range of T_{eff} for the sake of deriving synthetic colour- T_{eff} relations at various gravities and metallicities; or from theoretical isochrones as discussed in more detail further below.

Since one of the main uses of a library of bolometric corrections is to transform isochrones from the theoretical to various observational planes, we have provided an example of a computer code that will automatically select, and interpolate in, the appropriate `bc_***.data` file for the value of $[\alpha/\text{Fe}]$ that was assumed in the computation of the stellar models. This program, which has been given the name `iso2cmd.for`, must be compiled and linked with the interpolation subroutines in `bcutil.for` in order to produce an executable module. Although it currently assumes that the input isochrones are given in the format of the Victoria-Regina (hereafter VR) models by VandenBerg et al. (2014), those who wish to use the published grids of other workers should find it easy to modify `iso2cmd.for` to accommodate the format in which they have been presented.

Suppose that the `bc_***.data` files contain the BCs that were generated for the case that is the subject of Figures A1 and A2. The application of those transformations to two different VR isochrones

```

>iso2cmd
                                Input Isochrone File: a0zz_p4y25m16.iso
                                Default Iso-CMD file: [a0zz_p4y25m16.cmd]:
bc_p04 BCs for E(B-V) = 0.035 interpolated to [Fe/H] = -1.60
                                filters: F560W F1280W g i

>iso2cmd
                                Input Isochrone File: a0zz_p2y25m075.iso
                                Default Iso-CMD File: [a0zz_p2y25m075.cmd]:
                                *** a0zz_p2y25m075.cmd ALREADY EXISTS ***
                                Do you want to OVERWRITE? y
bc_m04 BCs for E(B-V) = 0.035 interpolated to [Fe/H] = -0.75
                                filters: F560M F1280M g i
bc_p00 BCs for E(B-V) = 0.035 interpolated to [Fe/H] = -0.75
                                filters: F560M F1280M g i
bc_p04 BCs for E(B-V) = 0.035 interpolated to [Fe/H] = -0.75
                                filters: F560M F1280M g i
>

```

Figure A3. Sample executions of `iso2cmd` in which the BCs that were generated by `get4bctables` (see the previous figure) have been applied to two different isochrones. These examples are explained in detail in the text.

is illustrated in Figure A3. If the executable module has been given the name `iso2cmd`, entering this name at the prompt will generate a request for the name of the input isochrone. In the first example, the name `a0zz_p4y25m16.iso` has been entered after the colon. By convention (see the Appendix in VandenBerg et al. 2014), `a0` refers to the solar mix of heavy elements derived by Asplund et al. (2009), `zz` specifies the entire group of α -elements, and the rest of the isochrone name indicates that $[\alpha/\text{Fe}] = +0.4$ (`_p4`), $Y = 0.25$ (`Y25`), and $[\text{Fe}/\text{H}] = -1.6$ (`m16`). (Had the models been computed for $[\alpha/\text{Fe}] = -0.4$, the first 7 characters of the isochrone name would have been `a0zz_m4`.) After the input isochrone has been identified, `iso2cmd` suggests that the output file be given the same name, but with the extension `.cmd` (see the third line of Figure A3). If that name is satisfactory, the user simply has to click on the “enter” key (without typing anything); otherwise, a different name (e.g., `testcmd.dat`) can be entered. The last two lines in `bc_p04.data`, which assume $E(B - V) = 0.035$, to obtain the reddening-corrected BCs at $[\text{Fe}/\text{H}] = -1.60$ for the filters `F560W`, `F1280W`, `g`, and `i`.

In the second example, an isochrone for $[\alpha/\text{Fe}] = 0.2$, $Y = 0.25$, and $[\text{Fe}/\text{H}] = -0.75$ (`a0zz_p2y25m075.iso`) is similarly transformed to the observed plane. If, as this in this case, a `.cmd` file of the same name already exists, the code issues a warning when the “enter” key is pressed to accept the default name, and the user is given the option of overwriting that file. By entering `y` (or yes), that option is accepted. (Had `n` or no been entered, the user would have been asked to provide an alternative name for the output file.) Because the value of $[\alpha/\text{Fe}]$ does not lie on the “standard” relation between $[\alpha/\text{Fe}]$ and $[\text{Fe}/\text{H}]$, it is necessary to perform interpolations in the `bc_m04.data`, `bc_p00.data`, `bc_p04.data` tables. Doing so yields the BCs for $[\alpha/\text{Fe}] = -0.4$, 0.0 , and $+0.4$, at $[\text{Fe}/\text{H}] = -0.75$; consequently, a further interpolation is carried out in these results to obtain the transformations at $[\alpha/\text{Fe}] = +0.2$ at the same metallicity.

Figure A4 reproduces the first two dozen lines in the `a0zz_p2y25m075.cmd` file that would have been generated in the second of the two test cases just described. The first 9 of the header lines list the number of isochrones, the assumed $[\text{Fe}/\text{H}]$ value and the initial $[m/\text{Fe}]$ ratios of the most important light elements, the initial mass-fraction abundances of the metals (Z), hydrogen (X), and helium (Y), the name of the metals mixture (`a0zz_p2`), and the

ISOCRONES	1
[Fe/H]	-0.750
[C,N,O/Fe]	0.00 0.00 0.20
[Ne,Na,Mg,Al/Fe]	0.20 0.00 0.20 0.00
[Si,S,Ca,Ti/Fe]	0.20 0.20 0.20 0.20
Z	3.327D-03 Mix: a0zz_p2
X	7.466498D-01
Y	2.500000D-01
ALPHA(mlt)	2.007
Solar number-fraction abundances for this mixture	
H 3He 4He 12C 13C	9.248160D-01 9.276509D-06 7.421207D-02 2.461821D-04 2.735357D-06
N O Ne Na Mg	6.262524D-05 4.529553D-04 7.871461D-05 1.607146D-06 3.681759D-05
Al Si P S Cl	2.606486D-06 2.992646D-05 2.377143D-07 1.219145D-05 2.924525D-07
Ar Ca Ti Cr Mn	2.323033D-06 2.023277D-06 8.242431D-08 4.036968D-07 2.489174D-07
Fe Ni 7Li 6Li 9Be	2.924525D-05 1.534813D-06 1.888232D-09 1.499876D-10 2.432514D-11

Age Npts E(B-V) = 0.035 is assumed in the Bolometric Corrections	
10.00 396	MIRIvega MIRIvega PanSTARR PanSTARR
Mass	log Te log g M_bol F560W F1280W g i
1 0.1200000000	3.501762 5.2321 11.63754 3.1643 3.3178 -2.9937 -0.3228
2 0.1250000000	3.505915 5.2192 11.51940 3.1434 3.2908 -2.9079 -0.2945
3 0.1300000000	3.509852 5.2066 11.40609 3.1234 3.2651 -2.8299 -0.2691
4 0.1350000000	3.513514 5.1946 11.29848 3.1045 3.2411 -2.7602 -0.2467
5 0.1400000000	3.516848 5.1833 11.19743 3.0871 3.2193 -2.6990 -0.2272

Figure A4. The first 24 lines in the output `.cmd` file of the $[\text{Fe}/\text{H}] = -0.75$ isochrone that was considered in the previous figure. The text contains a brief explanation of the information that is listed.

solar-calibrated value of the mixing-length parameter. The next 6 lines give the solar number-fraction abundances that are used by the Victoria stellar structure code to evaluate the surface $[m/\text{H}]$ and $[m/\text{Fe}]$ of the most abundant metals along evolutionary tracks. They are followed by the listing of the properties of individual models along a 10.0 Gyr isochrone (specifically, the mass in solar units, $\log T_{\text{eff}}$, $\log g$, M_{bol}), together with the reddening-corrected BCs for the indicated value of $E(B - V)$ and the 4 filters that are identified.

The absolute magnitude in any filter ζ can be determined from $M_{\zeta} = M_{\text{bol}} - BC_{\zeta} = -2.5 \log \frac{L}{L_{\odot}} + M_{\text{Bol},\odot} - BC_{\zeta}$, where L is the luminosity at a given T_{eff} , $\log g$ and $[\text{Fe}/\text{H}]$, and we refer to Section 3 for a discussion on the adoption of solar bolometric magnitude and luminosity. Differences in absolute magnitudes, $M_{\zeta} - M_{\eta}$, or equivalently, differences in the relevant bolometric corrections, $BC_{\eta} - BC_{\zeta}$ (note the reversal in the subscripts), then correspond to the predicted colour index $\zeta - \eta$. Although the header lines are specific to the VR computations, users should find it easy to produce equivalent listings (lines 17–) of isochrones produced by other workers with no more than a small amount of editing of `iso2cmd.for`.

APPENDIX B: EXTINCTION COEFFICIENTS

As discussed in length in Paper I, in presence of a given extinction the colour excess varies with stellar spectral type. This effect can be quite dramatic, and our interpolation routines allow for its exact treatment. However, there can be instances where for practical purposes the assumption of an average extinction coefficients is sufficient, or where the variation of extinction coefficients can be described with sufficient accuracy as function of T_{eff} and $[\text{Fe}/\text{H}]$. Table B1 provides extinction coefficients for the photometric systems studied in this paper, determined in the same manner as those reported in the analogous table included in Paper I.

Table B1. Extinction coefficients relevant to turnoff stars with $T_{\text{eff}} \lesssim 7000 \text{ K}^a$. Both mean extinction coefficients $\langle R_\zeta \rangle$, along with a linear fit of R_ζ as function of effective temperature and metallicity are provided.

Filter	$\langle R_\zeta \rangle$	$R_\zeta = a_0 + T_4 (a_1 + a_2 T_4) + a_3 [\text{Fe}/\text{H}]$				Filter	$\langle R_\zeta \rangle$	$R_\zeta = a_0 + T_4 (a_1 + a_2 T_4) + a_3 [\text{Fe}/\text{H}]$			
		a_0	a_1	a_2	a_3			a_0	a_1	a_2	a_3
JWST - MIRI											
<i>F560W</i>	0.102	0.1061	−0.0132	0.0102	—	<i>F770W</i>	0.102	0.0986	0.0106	−0.0088	—
<i>F1000W</i>	0.102	0.0964	0.0170	−0.0135	—	<i>F1130W</i>	0.102	0.0975	0.0140	−0.0115	—
<i>F1280W</i>	0.102	0.1081	−0.0204	0.0166	—	<i>F1500W</i>	0.102	0.1073	−0.0171	0.0134	—
JWST - NIRC <i>am</i>											
<i>F070W</i>	2.314	2.2385	0.1738	−0.0803	0.0010	<i>F090W</i>	1.514	1.4447	0.1833	−0.1125	—
<i>F115W</i>	1.011	0.9910	0.0313	0.0018	—	<i>F140M</i>	0.727	0.7233	0.0051	0.0011	—
<i>F150W2</i>	0.700	0.4673	0.5534	−0.2778	0.0023	<i>F150W</i>	0.663	0.6425	0.0454	−0.0189	0.0006
<i>F162M</i>	0.574	0.5719	0.0032	—	—	<i>F182M</i>	0.471	0.4709	0.0009	−0.0007	—
<i>F200W</i>	0.425	0.4159	0.0261	−0.0195	—	<i>F210M</i>	0.382	0.3747	0.0260	−0.0218	—
<i>F250M</i>	0.287	0.2828	0.0131	−0.0109	—	<i>F277W</i>	0.253	0.2554	−0.0086	0.0085	—
<i>F300M</i>	0.216	0.2222	−0.0175	0.0131	—	<i>F322W2</i>	0.214	0.2059	0.0254	−0.0189	—
<i>F335M</i>	0.179	0.1774	0.0056	−0.0045	—	<i>F356W</i>	0.166	0.1699	−0.0102	0.0075	—
<i>F360M</i>	0.158	0.1597	−0.0047	0.0036	—	<i>F410M</i>	0.132	0.1349	−0.0108	0.0092	—
<i>F430M</i>	0.121	0.1313	−0.0335	0.0267	—	<i>F444W</i>	0.119	0.1270	−0.0246	0.0200	—
<i>F460M</i>	0.106	0.1103	−0.0129	0.0106	—	<i>F480M</i>	0.101	0.0987	0.0083	−0.0075	—
SkyMapper											
<i>u</i>	4.900	3.3743	4.5098	−3.2967	−0.0193	<i>v</i>	4.550	4.3395	0.7243	−0.6196	−0.0028
<i>g</i>	3.446	2.9349	1.2782	−0.7275	−0.0054	<i>r</i>	2.734	2.6011	0.2952	−0.1284	—
<i>i</i>	1.995	1.9686	0.0394	0.0069	—	<i>z</i>	1.468	1.3831	0.2551	−0.1886	—
Tycho											
<i>H_P</i>	3.239	2.0611	2.9605	−1.6990	−0.0133	<i>B_T</i>	4.222	3.6609	1.6185	−1.1570	−0.0126
<i>V_T</i>	3.272	3.0417	0.5745	−0.3231	−0.0015						
Pan-STARRS1											
<i>g</i>	3.666	3.1864	1.2310	−0.7350	−0.0060	<i>r</i>	2.709	2.6161	0.2086	−0.0928	—
<i>i</i>	2.108	2.0702	0.0806	−0.0291	—	<i>z</i>	1.609	1.5920	0.0421	−0.0236	—
<i>y</i>	1.338	1.3078	0.0959	−0.0759	—	<i>w</i>	2.824	1.9382	1.9907	−0.8899	−0.0053
<i>o</i>	2.594	1.3963	2.6716	−1.1671	−0.0049						

^a Based on the differences in the bolometric corrections for $E(B - V) = 0.0$ and 0.10 , assuming $\log g = 4.1$, $5250 \leq T_{\text{eff}} \leq 7000 \text{ K}$, and $-2.0 \leq [\text{Fe}/\text{H}] \leq +0.25$, with $[\alpha/\text{Fe}] = -0.4, 0.0$ and 0.4 at each $[\text{Fe}/\text{H}]$ value. Note that (i) $T_4 = 10^{-4} T_{\text{eff}}$ in the fitting equation for R_ζ , and (ii) for a nominal $E(B - V)$, the excess in any given $\zeta - \eta$ colour is $E(\zeta - \eta) = (R_\zeta - R_\eta)E(B - V)$, while the attenuation for a magnitude m_ζ is $R_\zeta E(B - V)$. Also see the discussion in Paper I.